USING HIGH-RESOLUTION IMAGES TO ANALYZE THE IMPORTANCE OF CROWN SIZE AND COMPETITION FOR THE GROWTH OF TROPICAL TREES

Abstract

The influence of canopy structure on tropical tree growth has been scantly studied because of the difficulties making field measurements in these dense multi-layered ecosystems. The recent advent of unmanned aerial vehicles (UAVs), has made it easier to collect canopy data, so offering a way to gain a better understanding of forest productivity and thereby improve forest management. In this study, we assessed tree growth prediction using UAV-derived crown measurements as an alternative for field data.

Four experimental 9 ha plots were sampled in two forest sites, Yoko in the Democratic Republic of the Congo and Loundoungou in the Republic of Congo. Field inventories were made between 2015 and 2020. For each tree, we computed the diameter increment (DBHI) using censuses and diameter-based competition indices (diameter-based CIs) using the first census. High-resolution orthoimages and digital surface models were acquired with UAVs in 2016 and 2018 in the two sites. They gave estimates of crown characteristics (size, relative elevation, shape) and crown-based competition indices (crown-based CIs). Co-recorded UAV and field measurements were obtained for 1558 trees. The diameter increment of these trees was then modelled using supervised component generalized linear regression, and 20% of trees were kept for cross-validation.

Combined field and UAV data predicted tree DBHI twice better than either taken separately. Diameter at breast height (DBH) and crown area (CA) were found to be complementary predictors.

Crown-based CIs significantly improved predictions of models already containing DBH and CA. Adding diameter-based CIs to models containing DBH, CA, and crown-based CIs only marginally improved growth predictions, showing that tree competition can be well-described with UAV data. The model calibrated at one site predicted the growth at the other site well, suggesting that a general model could be devised for multiple sites. Growth variance was better explained in the site (Yoko) where the crown density was higher and the crown smaller. Further data are now needed from multiple sites with ranging stand structures and compositions to build a general model.

Keywords: Tropical forest, canopy structure, crown competition, drone, tree growth modelling

1. INTRODUCTION

Tree growth is an intermittent process that brings changes in stem shape and size (Guerra-Hernández et al., 2017). Reliable data on tree growth and a better understanding of its drivers are needed in many tropical forests (Rozendaal et al., 2020) to predict future stand composition (Rüger et al., 2011), calibrate dynamics models (Purves and Pacala, 2013), assess carbon sequestration (Rutishauser et al., 2010), and develop decision support tools to guide forest management (Burkhart and Tomé, 2012).

Tree growth is highly variable. It depends on numerous drivers and it is then challenging to model it in complex forests. Stem diameter increment depends on a tree's life history, genetic heritage – reflecting the evolutionary history and adaptation of the parent population to different environments – and ontogenic stage, expressed in terms of age or size (Prévosto, 2005). It also depends on tree species and functional traits, and on the availability of on-site resources (light, water, and nutrients), which may be depleted by competing species in dense stands (Baker et al., 2003; Davies, 2001). In general, the adverse effects of competition on tree growth depend on the size of the subject trees and on their tolerance to competition and shading, and on how crowded the local neighborhood is (Rozendaal et al., 2020; Uriarte et al., 2004). For any given species, small trees are often the most severely affected by competition, and light-demanding species are often highly responsive to changes in competition intensity (Kunstler et al., 2016; Uriarte et al., 2004).

For a given subject tree, competition is often assessed indirectly using competition indices. The competition for resources can be either size-symmetrical or size-asymmetrical, depending on how it affects trees of different sizes. Size-symmetrical competition occurs when the effect of competition is proportional to tree size. Size-asymmetrical competition occurs when the effects are more than proportional tree size (Rasmussen and Weiner, 2017; West and Ratkowsky, 2021). In most growth models developed in tropical forests, competition indices have been based on diameter and/or height of neighbors (Franc et al., 2000). In some cases, competition indices are functions of distances between trees (distance-dependent). In others, the indices do not take into account the position of the measured trees (distance-independent) (Biging, 1995). Neighboring trees are usually defined as standing within a circular zone of influence of set radius, generally between 3 m and 30 m (Barros de Oliveira et al., 2021; Gourlet-Fleury and Houllier, 2000; Gourlet-Fleury et al., 2023).

Competition indices can be a function of the size and position of neighboring tree crowns as demonstrated in temperate forests (Cole and Lorimer, 1994; Schomaker et al., 2007; Wyckoff and Clark, 2005; Zarnoch et al., 2004). However, this approach has been rare in dense tropical forests (but see Foli et al., 2003; Franc et al., 2000) because crown measurements are particularly difficult to make and imprecise in multi-layered forests, especially for large trees (Blanchard et al., 2016). One of the few reported studies in tropical forests using field-derived crown measurements (Zambrano et al., 2019) recently showed the importance for growth and mortality predictions of competition indices based on crown overlap and neighboring trees being taller than the subjects. Such crown measurements attempt to measure, even indirectly, the amount of light intercepted by the tree, which is one of the main factors limiting growth for tropical trees (Baker et al., 2003). Therefore, crown indices are expected to provide more accurate and reliable indicators of tree growth and productivity in tropical forests than diameter-based indices.

In the last few decades, airborne laser scanning (ALS) and digital aerial photogrammetry (DAP) have supplied detailed information on tree crowns (Järnstedt et al., 2012), first in temperate forests (Popescu et al., 2003) and more recently in tropical forests, following with the advent of unmanned aerial vehicles (UAVs) (Getzin et al., 2012; Paneque-gálvez et al., 2014). RGB sensors can now be mounted on inexpensive UAV platforms that offer high operational flexibility, with low flight costs and the ability to take off *in situ* and fly at low altitude under cloud cover, enabling very high-resolution 3D imaging in forests inaccessible from the ground (Messinger et al., 2016). Several studies have recently shown excellent results for DAP applications in estimating canopy structure (Bourgoin et al., 2020) and stand productivity (Price et al., 2020; Tompalski et al., 2021). However, data collected with UAVs have rarely been used to assess tree growth even though this variable is critical for forest management (Guerra-Hernández et al., 2017). High-resolution UAV images can be used to identify, delineate, and measure individual tree crowns. Many variables related to crown size, shape and position can be extracted (Getzin et al., 2012; Ndamiyehe et al., 2020) and added to classical field measurements such as stem diameter and social status (Moravie et al., 1999).

Though requiring new technological and analytical resources, the reduced operational cost and the high resolution of UAV imagery offer opportunities to replace or complement field measurements, which are particularly time-consuming and difficult in tropical forests. UAV imagery also offers the possibility to repeat canopy measurements at close intervals to monitor and detect fine changes of forest structure (Tompalski et al., 2021).

In this study, we set out to explore the possibility of extracting new crown variables from UAV images and to assess whether those variables could improve tree growth predictions. We specifically addressed the following questions.

1. Can UAV images help detect differences in stand structure across sites?
2. Can crown-based competition indices replace stem diameter-based competition indices to predict tree growth?
3. Can a general model of tropical tree growth be derived that works for multiple sites?

We fitted different models of tree diameter increment in response to multiple crown-based and stem diameter-based competition indices to assess the use of UAV data. The models were fitted with supervised component-based generalized linear regression 'SCGLR' (Bry et al., 2013), a robust method to compare models in which many correlated explanatory variables are tested (Réjou-Méchain et al., 2021; Tomaschek et al., 2018).

2. MATERIALS AND METHODS

2.1 Study sites

The study was conducted in two sites of intact forest (not logged in the past) in central Africa (Fig. 1), Yoko and Loundoungou. The Yoko site, in the Democratic Republic of the Congo (DR Congo), is located 32 km southeast (0°17'N, 25°18'E) of Kisangani and characterized by a mean annual temperature of 25°C, a mean annual precipitation of 1750 mm, and no dry months (Picard et al., 2015). The soils are oxisols and the average elevation is 450 m. The Loundoungou site is located in the north of the Republic of Congo (2°24' N, 17°05'E), where the average temperature is 25°C. The average rainfall is 1600 mm and there is a dry season from December to March, with two dry months (December and January). The topography is slightly uneven, with an average elevation of 430 m. The geological substrate consists of alluvial deposits (Fayolle et al., 2014; Ligot et al., 2022; Loubota Panzou et al., 2018). The vegetation in both sites is moist Central African (Fayolle et al., 2014), specifically of the semideciduous type for Loundoungou and semideciduous evergreen transition type for Yoko (Fig. 1, Réjou-Méchain et al. (2021)). In Yoko, the area surrounding the study site is dominated by agricultural fields and forest patches of secondary and degraded woodlands. In Loundoungou, the area surrounding the study site is dominated by forests that have been little affected by human activity.

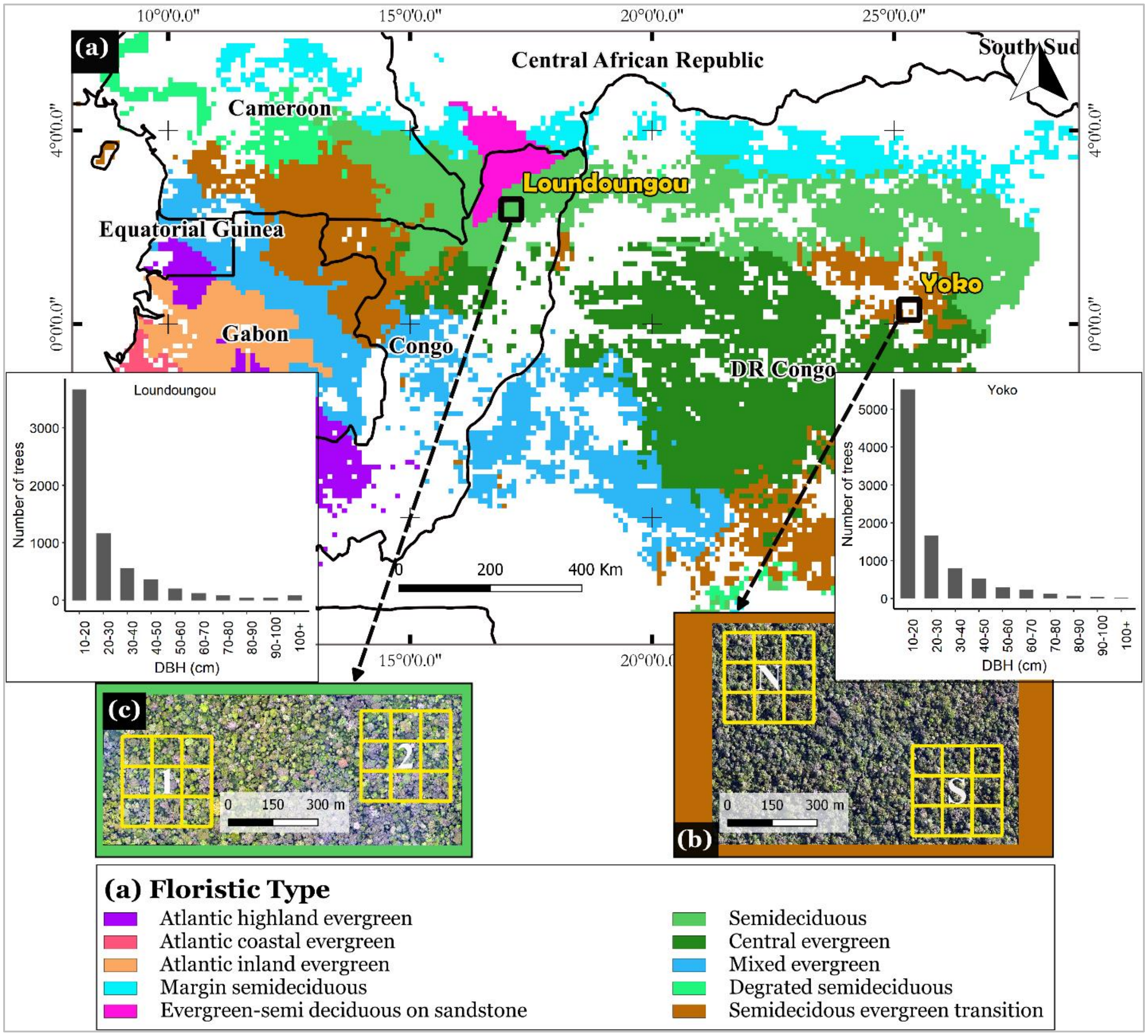

Fig. 1. Location of the Yoko (Democratic Republic of the Congo) and Loundoungou (Republic of Congo) sites across (a) forest types (Réjou-Méchain et al., 2021). The experimental plots (yellow) in (b) Yoko and in (c) Loundoungou are presented with UAV images in the background. The diameter class distributions of trees inventoried in 2018 are also shown for each site.

2.2 Field inventory data

In each site, two experimental plots of 9 ha were sampled (Fig. 1) following a standardized protocol (Picard and Gourlet-Fleury, 2008). Within each plot, we measured all trees with a diameter at breast height (DBH) ≥ 10 cm. For each measured tree, we recorded botanical identity and spatial coordinates, and we measured the diameter with a tape. In both sites, tree diameter was measured twice between 2015 and 2020 (Table 1). Diameter increments (DBHIs) were computed over a minimum of two years. A total of 351 distinct species were identified, of which 88 were present in both sites. On average, 450 trees. ha^{-1} were measured in Yoko and 350 trees ha^{-1} in Loundoungou. The five common dominant families in the two sites were *Fabaceae, Meliaceae, Euphorbiaceae, Annonaceae,* and *Myrticaceae.* These species made up 51% and 30% of trees in Yoko and Loundoungou, respectively.

2.3 UAV images

Aerial photographs were acquired using fixed-wing UAVs equipped with RGB sensors (Table 1). The flight plans were prepared (altitude and overlap of photographs) and executed in the Mission Planner version 1.3.31 environment. Overlaps between flight bands and between line bands were set at 80% for all flights to allow optimal alignment of photographs. The photographs were then processed in the Agisoft Photoscan environment (PhotoScan, 2015). The processing has three main steps: (i) camera calibration to mitigate the positioning errors of the UAV during image capture, (ii) image alignment by automatic matching of common points identified on neighboring images, and (iii) 3D canopy scene reconstruction (Lisein et al., 2013; Michez et al., 2016). We then obtained georeferenced orthoimages with a resolution of 10 cm pixel^{-1} and digital surface models (DSMs) with a resolution of 30 cm pixel^{-1}. The images covered the area of the experimental plots plus a 50 m-wide buffer area around them (Fig. 2a). Given the uneven terrain and the difficulty to collect ground points due to the dense vegetation in the two sites, we were unable to calculate the digital terrain model (DTM). As a result, we could not apply a standard method (DSM-DTM) to derive the digital height model.

Table 1. Field inventory and UAV acquisition data in the two sites and four plots: Yoko (northern plot N and southern plot S) and Loundoungou (Plots 1 and 2).

	Field inventory		UAV image acquisition			
Site	Period	DBH ≥ 10 cm in 2018	Period	UAV	Camera	Area covered
Yoko	N: 2018-2020	5446 trees, 196 species	June 05, 2016	Wingspan: 2.5 m	Brand: Sony Nex7	400 ha
	S: 2015-2019	4375 trees, 188 species		Weight: 6 kg	Resolution: 24.1 MP	
	Plots N + S	9821 trees, 223 species			Lens: 16 mm	
Loundoungou	1: 2015-2018	2968 trees, 190 species	June 18, 2018	EBEE 03-907	Brand: S.O.D.A.	1 400 ha
	2: 2015-2018	3396 trees, 192 species		Wingspan: 0.96 m	Resolution: 20 MP	
	Plots 1 + 2	6364 trees, 216 species		Weight: 0.69 kg	Lens: 13.133 mm	

2.4 Delineation of tree crowns and co-recording with field data

To link UAV data with field inventory data, the positions of trees surveyed in the field were matched with the positions of tree crowns detected on UAV images by the co-recording approach described in Ndamiyehe et al. (2020). First, the tree stem positions defined in a local reference frame were transformed into the image coordinate system. A sample ($n \geq 10$) of dominant non-tilted trees was selected, spotted on the *in situ* orthoimages using a Microsoft Surface Pro 7 tablet (www.microsoftsurface.com) with QGIS software. Matching the tree stem and crown centroid positions of these dominant trees thus enabled us to apply an affine transformation (Carrillo, 2015) to the local coordinates of all the trees in the plot and to obtain their UTM coordinates. The centroids of the tree crowns were then considered as estimators of the position of the tree apex. Since these two positions may be offset, we rectified the positions of all canopy trees (2630) with respect to their crown centroids (Table 2). The crowns present on each of the four sampled plots together with those inside a 50 m-wide buffer area around the plots (Fig. 2a) were manually delineated in the QGIS Development Team (2020). To locate tree crowns more precisely, they were examined on both the orthoimages and the DSMs. Translation was then carried out between trees and their nearby crown centroid, followed by a field check. The delineation of the crowns took approximately 21 days of 8 hours work. The co-recording of the trees and the field verification required approximately 13 additional days.

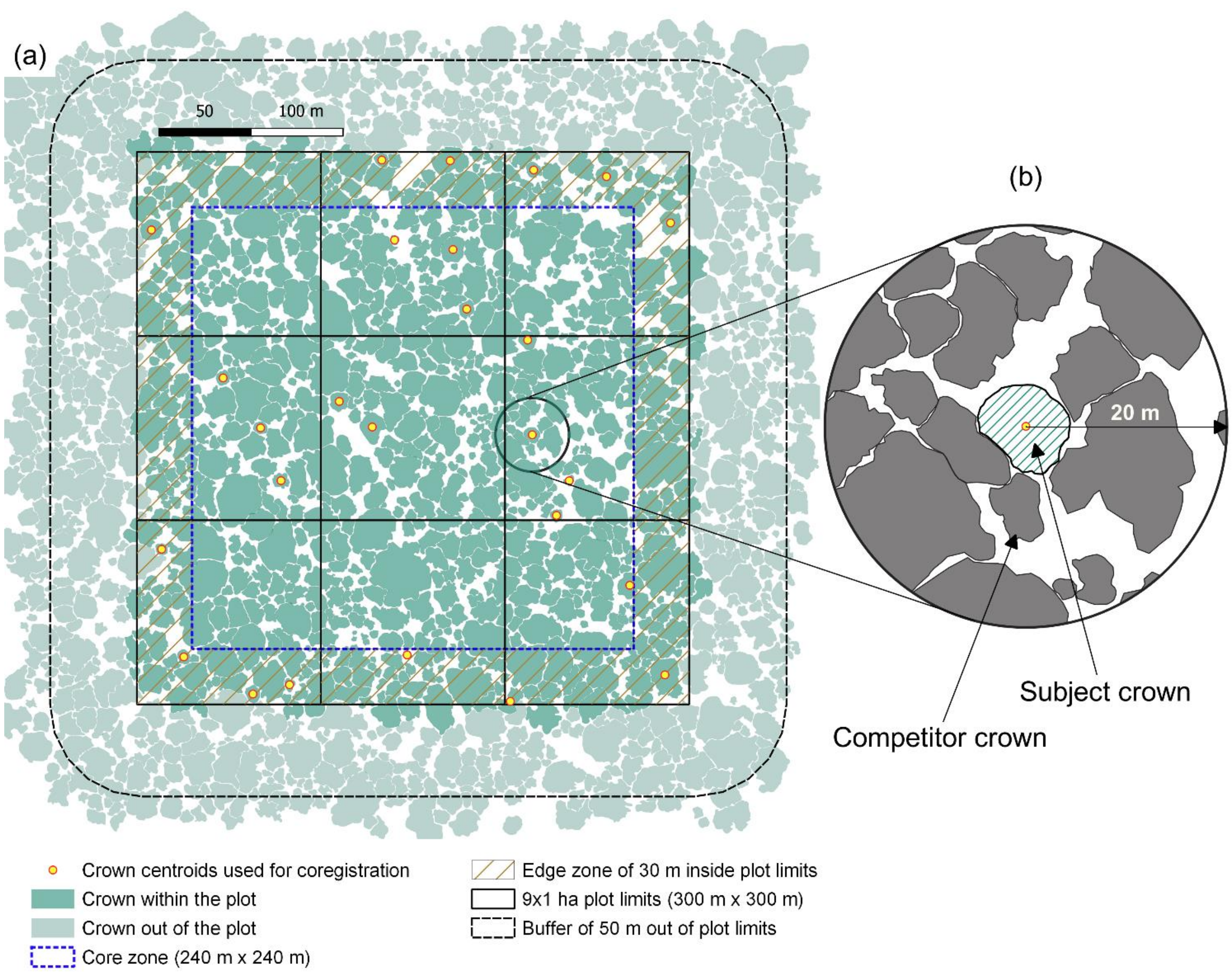

Fig. 2. Delineation of tree crowns (a) within one of the four sampled plots and within a 50 m-wide buffer zone (black dashed boundary). DBH-based competition indices were calculated only for the trees in the

core zone. Crown-based CIs (b) could be computed for the trees in the buffer zone of the plot also. Competition indices were computed for different zones of influence centered on the subject tree. For an example zone of influence of 20 m, the neighborhood crowding index (NCI), one of the computed competition indices, is the ratio of the subject crown area to the cumulative area of competitor crowns (black area).

2.5 Data analysis

2.5.1 Variables measured from field surveys and aerial images

Crown size (crown area, crown perimeter, and crown diameter), crown shape (crown circularity and ratio of crown perimeter to crown area, Getzin et al., 2012) and crown relative position within the canopy were computed from the orthoimages and DSMs obtained by UAV. The relative canopy position was calculated as the difference between the subject tree's altitude and its neighborhood altitude (ΔALT). As the effect of a tree on its neighborhood can operate over ranging distances depending on the tree's size and species, several neighborhood zone areas were considered (Fig. 2). In this study, ten radii of interval 2.5 m were tested, giving for each tree ten values of ΔALT over a maximum radial distance of 25 m (Laurans et al., 2014). The mean ΔALT over the ten radii was taken to determine the categorical variable (crown situation, CR_{SITU}), characterizing the location of a given crown in relation to the canopy, distinguishing dominated crowns ($\Delta ALT < 0$) from dominant crowns ($\Delta ALT \geq 0$).

The size of each crown was computed either as the orthogonal crown projection area (CA) or as the convex crown area (CCA) using orthoimages. Hybrid variables were then computed by dividing these crown variables by the basal area (BA) of the subject tree measured with field data. The hybrid variable was expected to capture the recent growth strategy of trees, notably the trade-off between crown expansion and diameter growth for trees released in the canopy (Antin et al., 2013; Blanchard et al., 2016). By using a hybrid variable, we hypothesize that, at a given DBH, trees with larger crowns exhibit higher diameter growth rates due to their enhanced photosynthetic capacity (Ndamiyehe et al., 2020; Wyckoff and Clark, 2005).

Overall solar radiation was also estimated for each crown with the r.sun.insoltime algorithm from GRASS software (Hofierka and Suri, 2002; Olpenda et al., 2018) considering the DSM as the input layer. Global solar radiation was calculated for the first day of each month, and an annual average was then computed (glob_rad in Wh m^{-2} day^{-1}).

To account for species shade tolerance, a regeneration guild *sensu* Hawthorne (1995) was assigned to each species from Bénédet et al. (2013): contrasting pioneer, non-pioneer light-demanding (NPLD), and shade-tolerant (SB). Finally, the variable stem size class (S_{SIZE}), distinguished large trees (DBH ≥ 40 cm) from small trees (DBH < 40 cm).

2.5.2 Competition indices from both field and images

Competition indices (CIs) using field data (Table 2) are classically used in tropical forests (Gourlet-Fleury and Houllier, 2000; Moravie et al., 1999) and were calculated here in circular zones of radius 5, 10, 15, 20, 25, and 30 m. The DBH-based CIs were calculated only for trees located in the core zone of the plot. For the trees in the edge zone, the CIs could not be computed as their zone of influence (of maximum radius of 30 m) had not been fully inventoried. However, the crown-based CI were calculated for trees located in the entire plot area (core plus edge zones, Fig. 2a), given that the ortho-images acquired extended 50 m outside the plot boundaries. Taking into account the distance and size of competitors, four group of indices could be recognized: (i) distance-dependent symmetrical competition indices, (ii) distance-dependent asymmetrical competition indices, (iii) distance-independent symmetrical competition indices, and (iv) distance-independent asymmetrical competition indices. The symmetric competition indices included all identified neighbors in the zone of influence. In contrast, asymmetric competition indices were calculated by considering as competitors of a given subject tree only the neighboring trees with larger and/or taller crowns than the subject (Rio et al., 2014; West and Ratkowsky, 2021). Ten indices were computed with Equation 1. Competition indices other than those described with Equation 1 were calculated, and formulas are given in Table 2.

$$\mathrm{CI}_i = \sum_{j=1}^{n} \mathrm{CA}_j^{\alpha} / \mathrm{DIST}_{ij}^{\beta}, \qquad \text{Eq. 1}$$

where CI_i is a competition index for subject tree i depending on the crown area (CA_j) of the n neighboring trees located at distance DIST_{ij} from the subject tree. Exponents α and β could be set to 0, 1 or 2 to weight CA and/or DIST. If $\beta = 0$, the competition indices were distance-independent; otherwise, they were distance-dependent (Eq.1). If $\alpha = 0$ and $\beta = 0$, the resulting index corresponded to the number of neighboring trees within the influence zone. The indices were also computed considering all neighboring trees (symmetrical competition) or only the trees larger than the subject trees (asymmetrical competition).

Table 2. Variables and competition indices used to predict tree growth, measured or calculated from field data, UAV, or a combination of both (hybrid variables). DBH-based CIs are marked $^{\phi}$; crown-based CI are marked ‡. The Model column states, for each variable, the model including these variables among the predictors (see Section 2.5.3).

Variable type	Definition	Index	Formulas	Reference	Model
Field (DBH-based variables)	Diameter at breast height	DBH	—		M1,M3,M4,M5
	Logarithm of DBH	logDBH	Log(DBH)		M1,M3,M4,M5
	Logarithm of squared DBH	logDBH2	$\mathrm{Log(DBH)}^2$		M1,M3,M4,M5
	Logarithm of $(\mathrm{DBH})^{1/2}$	logDBH12	$\mathrm{Log(DBH)}^{0.5}$		M1,M3,M4,M5
	Stem size class	S_{SIZE}	DBH < 40 cm: small tree DBH ≥ 40 cm: large tree		M1,M3,M4,M5
	Number of neighbors$^{\phi}$	Nn	—		M1,M5
	Number of neighbors taller than the subject tree$^{\phi}$	NnT	—		M1,M5
	Sum of the basal areas of the neighbors$^{\phi}$	SBA	$\sum_{i=1}^{Nn} \pi/4 \times \mathrm{DBH}_i^2$	Moravie et al. (1999)	M1,M5
	Sum of the basal areas of the taller neighbors$^{\phi}$	SBAT	$\sum_{i=1}^{NnT} \pi/4 \times \mathrm{DBH}_i^2$		M1,M5
	Basal area ratio$^{\phi}$	BAR	BA/(BA+SBA)	Moravie et al. (1999)	M1,M5
Remote sensing (UAV-based variables)	Projected crown area	CA	—		M2,M3,M4,M5
	Logarithm of crown area	logCA	Log(CA)		M2,M3,M4,M5
	Convex crown area	CCA	$\sum_{i=1}^{n} \frac{S_i}{\min(\cos(\mathrm{slope}_i))}$	Ndamiyehe et al. (2020)	M2,M3,M4,M5
	Crown diameter	CD	$(4 \times \mathrm{CA}/\pi)^{0.5}$		M2,M3,M4,M5
	Crown perimeter	CP	—		M2,M3,M4,M5
	Crown situation	CR_{SITU}	ΔALT < 0: dominated crown ΔALT ≥ 0: dominant crown		M2,M3,M4,M5
	Crown circularity	CCircu	$4\pi \times \mathrm{CA}/\mathrm{CP}_i^2$	Getzin et al. (2012)	M2,M3,M4,M5
	Crown perimeter / area ratio	CPA	CP/CA	Getzin et al. (2012)	M2,M3,M4,M5

	Difference in altitude between the subject tree and its neighborhood	ΔALT	—	Ndamiyehe et al. (2020)	M2,M3,M4,M5
	Number of all neighboring tree crowns⸙	NC	Eq. 1, with $\alpha = 0$, $\beta = 0$		M2,M3,M4,M5
	Number of neighboring crowns higher than the subject⸙	NCH	Eq. 1, with $\alpha = 0$, $\beta = 0$	Ma et al. (2018)	M2,M3,M4,M5
	Number of neighboring crowns larger than the subject	NCL	Eq. 1, with $\alpha = 0$, $\beta = 0$		M2,M3,M4,M5
	Neighboring crowns higher and larger than the subject⸙	NCHL	Eq. 1, with $\alpha = 0$, $\beta = 0$		M2,M3,M4,M5
	Sum of the crown area of neighboring trees⸙	NCA	$\sum_{j=1}^{\mathrm{NC}} \mathrm{CA}_j^{\alpha}/\mathrm{DIST}_{ij}^{\beta}$ with $\alpha = 1$, $\beta = 0$		M2,M3,M4,M5
	Neighborhood crowding index⸙	NCI	NCA/Area of influence zone		M2,M3,M4,M5
	Sum of the crown area of higher trees⸙	CAH	$\sum_{j=1}^{\mathrm{NCH}} \mathrm{CA}_j^{\alpha}/\mathrm{DIST}_{ij}^{\beta}$ with $\alpha = 1$, $\beta = 0$		M2,M3,M4,M5
	Sum of the crown area of larger trees⸙	CAL	$\sum_{j=1}^{\mathrm{NCL}} \mathrm{CA}_j^{\alpha}/\mathrm{DIST}_{ij}^{\beta}$ with $\alpha = 1$, $\beta = 0$	Filipescu et al. (2012)	M2,M3,M4,M5
	Sum of the crown area of higher and larger trees⸙	CAHL	$\sum_{j=1}^{\mathrm{NCHL}} \mathrm{CA}_j^{\alpha}/\mathrm{DIST}_{ij}^{\beta}$ with $\alpha = 1$, $\beta = 0$		M2,M3,M4,M5
	Distance weighted sum of the neighboring crown area⸙	NCA_{DW}	$\sum_{j=1}^{\mathrm{NC}} \mathrm{CA}_j^{\alpha}/\mathrm{DIST}_{ij}^{\beta}$ with $\alpha = 1$, $\beta = 1$		M2,M3,M4,M5
	Global solar radiation	glob_rad	—	Hofierka and Suri (2002) Olpenda et al., 2018)	M4
Hybrid	Ratio of projected crown area to basal area	CBR	CA/BA	Wyckoff and Clark (2005)	M4,M5
	Ratio of convex crown area to basal area	CCBR	CCA/BA	Ndamiyehe et al. (2020)	M4,M5

2.5.3 Growth models

To test whether the use of UAV data provided information similar or complementary to field data for predicting tree growth, we first analyzed the correlations between these two types of data using principal component analysis (PCA). We then tested the influence of the two types of data in growth models including all variables, even those potentially correlated. Five models were calibrated considering the trees located in the core of the plots (Fig. 2a, Table 2). Models 1 and 2 (M1 and M2) were calibrated using only field or UAV variables, respectively. Model 3 (M3) was calibrated using all variables except the hybrid variables. Model 4 (M4) was calibrated using the UAV-derived variables, the hybrid variables, and tree diameter (see Section 2.5). Model 5 (M5) contains all possible variables from the field, UAV and the hybrid variables. Comparing models M4 and M5 allowed us to quantify the importance of diameter-based CIs (absent in M4) in the presence of crown data. The categorical variables, namely the stem size class (S_{SIZE}), crown situation (CR_{SITU}) and species guild (TE), were added to the models (Table 2) as additional variables. To account for the non-linear relationship between tree growth and size (Hérault et al., 2011), stem and crown size were log-transformed (Gourlet-Fleury and Houllier, 2000). In addition, to homogenize the variance of the residuals, we used a logarithmic transformation of the response variable (DBHI). To avoid the problem of logarithms on negative increments, we used log(DBHI+1) instead of log(DBHI) (Gourlet-Fleury et al., 2023).

Given the large number of covariates and the strong correlations between them (Appendix A and see PCA results in Appendix B), we fitted supervised component generalized linear regressions (SCGLRs) (Bry et al., 2013) to take account of information redundancy in the bundles of variables. SCGLR identifies a reduced number of the most predictive components through linear combination of covariates (Table 2). The components are constructed by searching for the directions of high variance in the predictor space that at the same time are optimal for predicting the response variable (Réjou-Méchain et al., 2021; Tomaschek et al., 2018). To maximize the trade-off between goodness of fit and the amount of information the components capture from the covariates, three parameters must be defined cautiously: $l \geq 1$ measures the locality of the bundles of variables with which the components tend to align, s, between 0 and 1, describes the structural strength of the predictors, and k is the optimal number of model components (Bry et al., 2013; Mortier et al., 2017). These parameters were determined by cross-validation using the harmonic mean of the mean square prediction error (MSPE) criteria (Appendix C).

The predictive power of the models was tested with a cross-validation in which the dataset was randomly subdivided into a training dataset (80% of trees) and a validation dataset (20%). The model fitted on the training sample was tested to predict the growth of the trees in the validation sample. The operation was repeated 10 times and the mean coefficients of determination (R^2) and the mean square prediction error (MSPE) were used to quantify the accuracy of the models. The calculation of R^2 involved three steps: (i) the coefficients that form the components were calculated on the training sample, (ii) these coefficients were then used to calculate the components on the validation sample, and (iii) the response variable was regressed with least squares regression on these components in the validation sample, to obtain the R^2, adjusted R^2 (R^2 adj) and p-values.

The model with the best compromise between parsimony and accuracy was identified among M1–M5 based on their R^2 adj and MSPE values along with the type of variables and number of components it contained. This model was then tested at the two sites separately. To test the site effect, the model fitted to one site was tested to predict DBHIs on the other site and vice versa. We also fitted simple linear regression to detect significant variables in the best model. We started with a model including all possible explanatory variables. Then, we used an automatic procedure (stepAIC) to remove the variables one by one, based on the Akaike information criterion (AIC) to identify the best model in terms of AIC and parameter number.

UAV data were processed using QGIS software version 2.18 (QGIS Development Team, 2020) and different R packages: sf version 0.9.2 (Anderson and Winter, 2020), raster version 3.5-2 (Hijmans et al., 2020), qgisprocess version 0.0.0.9000 (Caha, 2023), and vec2dtransf version 1.1 (Carrillo, 2015). Statistical models were calibrated using the SCGRL packages version 3.0.9000 (https://github.com/SCnext/SCGLR/) and MASS version 7.3-54 (Venables et al., 2002). All statistical analyses were performed in R (R Core Team., 2021).

3. RESULTS

3.1 Using UAV data to describe canopy structure

A total of 4961 crowns were delineated on UAV images. Of these, 2630 were located within the 9 ha plots and 2331 in the 50 m buffer zones (Fig. 2). A total of 1558 delineated crowns were paired to trees identified in the field surveys: 984 were located in the core of the plots and 574 in the edge zones. The paired trees made up 9.6% of the inventoried trees (Table 2) and 38% of species (n = 135, Appendix G). The crown diameter of these paired trees was on average lower in Yoko (9.5 ± 4.8 m) than in Loundoungou (12.0 ± 5.6 m) (Appendix D) and this difference was significant ($t = -12.41$, df = 2628, $p < 0.001$). Within sites, the mean crown diameter did not vary significantly between plots (Yoko: $t = -0.39$, df = 1575, $p = 0.69$; Loundoungou: $t = 0.23$, df = 1051, $p = 0.82$). Differences in crown density were also observed between the two sites: crowns were significantly denser ($t = -7.74$, df = 34, $p < 0.001$) in Yoko (83.1 ± 9.9 crowns ha^{-1}) than in Loundoungou (56.2 ± 10.9 crowns ha^{-1}). The DBH of paired trees ranged between 10.3 cm and 204.1 cm, and 72% of them were more than 40 cm in diameter (see in Appendix H, the DBH distribution of sampled trees). Diameter increment varied across sites and species guild (Table 2). Trees grew faster in Loundoungou than in Yoko (ANOVA I: $F = 20.03$, df = 1556, $p < 0.001$).

Table 3. Number of inventoried trees, delineated crowns and co-recorded crowns together with the proportion of delineated and co-recorded crowns among the trees inventoried in 2018. The mean and standard deviation of stem diameter and diameter increment in cm year^{-1} in the two study sites (Yoko and Loundoungou) for co-recorded trees are also shown by site and species guild: pioneer, non-pioneer light-demanding (NPLD), and shade-tolerant (SB).

Site	Inventoried trees	Crown delineated	UAV-field data co-recorded	% of data co-recorded	DBH range of co-recorded trees (cm)	DBHI (cm year^{-1}) of co-recorded trees by species guild	
Yoko	9821	1577	876	8.9	10.3–160.4	Pioneer	0.983 ± 0.857 ($n = 88$)
						NPLD	0.421 ± 0.355 ($n = 276$)
						SB	0.297 ± 0.317 ($n = 512$)
Loun-doungou	6364	1053	682	10.7	10.3–204.1	Pioneer	0.842 ± 0.738 ($n = 129$)
						NPLS	0.494 ± 0.462 ($n = 229$)
						SB	0.404 ± 0.311 ($n = 324$)
Total	**16185**	**2630**	**1558**	**9.6**	**10.3–204.1**	—	—

3.2 Variable and model selection

According to the MSPE drop for the five fitted models, two supervised components (SC) were optimal for predicting growth (Fig. 3a) of the 984 trees studied in the core zones. Diameter increment (DBHI) was strongly correlated to these two first components (SC1 and SC2).

DBHI was negatively correlated with SC1, except in M1 (Fig. 3b). In contrast, DBHI was positively correlated with SC2 in all the models. Variables characterizing crown size (CA, CCA, CD), relative altitude (ΔALT) and tree diameter (DBH) were the most negatively correlated with SC1 and showed a positive effect on DBHI. Hybrid variables (CBR, CCBR) were also positively correlated with Axis 2 and showed the strongest correlation with DBHI, especially in Model 4 (Fig. 3e). Hybrid variables were also negatively correlated to the basal area of neighboring trees (SBA, BAR) (see also PCA results, Appendix B), showing that the greater the competition exerted on a tree, the smaller was the crown to basal area ratio. Both the SC1 and SC2 showed that in general, the asymmetric (NCL, NCHL) and symmetric (NCA, NCI, NC, Nn) competition indices assessed from field or UAV data at different radii negatively affected DBHI. When all field and UAV data were combined (M5, Fig. 3f), crown-based competition indices (CAHL, NCL, NCI,) were found to correlate better with SC1 and SC2, and therefore with DBHI, than the diameter-based competition indices (SBAT, NnT). The crown competition types that had the most influence on SC1 and SC2 were both symmetric (NC, NCI) and asymmetric (NCL, CAHL), and they varied in the size of the zone of influence where they were measured (Fig. 3f). The variables with the strongest correlations ($r \geq 0.60$) with the supervised components are given in Appendix E.

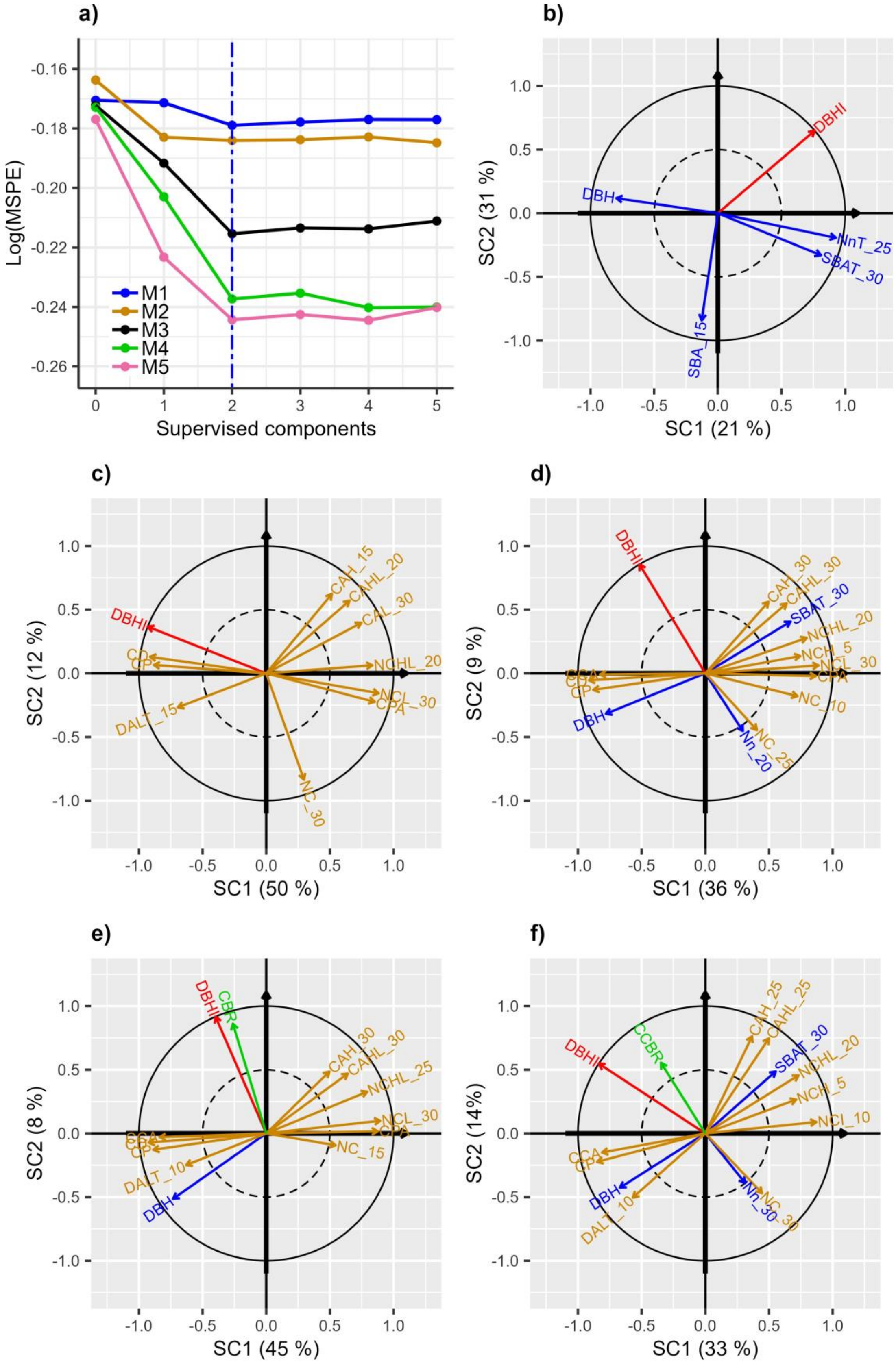
a)
Log(MSPE)
Supervised components
M1
M2
M3
M4
M5
b)
SC1 (21 %)
SC2 (31 %)
DBHI
DBH
NnT_25
SBAT_30
SBA_15
c)
SC1 (50 %)
SC2 (12 %)
DBHI
CAH_15
CAHL_20
CAL_30
NCHL_20
NCL
CSA_30
DALT_15
NC_30
CP
d)
SC1 (36 %)
SC2 (9 %)
DBHI
CAH_30
CAHL_30
SBAT_30
NCHL_20
NCH_5
NCL_30
CPA
NC_10
NC_25
Nn_20
DBH
CP
e)
SC1 (45 %)
SC2 (8 %)
DBHI
CBR
CAH_30
CAHL_30
NCHL_25
NCL_30
NC_15
DALT_10
DBH
CP
f)
SC1 (33 %)
SC2 (14%)
DBHI
CCBR
CAH_25
CAHL_25
SBAT_30
NCHL_20
NCH_5
NCI_10
CCA
CP
DBH
DALT_10
Nn_30
NC_30

Fig. 3. In (a), the optimal number of components in the fitted models is marked by the blue dotted lines analyzing the variation in mean square prediction error. Correlation plots for the predictors and response variable in the planes defined by the supervised components SC1 and SC2 are presented for the model fitted using variables from (b) field (Model 1), (c) UAV (Model 2), (d) field + UAV (Model 3), (e) DBH + UAV + hybrid (Model 4), and (f) the entire set of variables calculated in this study (Model 5). For clarity, variables with a correlation of less than 0.5 with both components (dashed circle) are not shown. Similarly, each competition index is represented by considering the zone of influence for which the index has the best correlation with the components. The predicted variable is shown in red, DBH-based variables in blue, UAV-based variables in orange and hybrid variables in green.

Comparison of the calibrated models considering data from the two sites combined (Fig. 3, Fig. 4a) or separated (Fig. 4b,c) showed the same trend: the predictive quality of M1 and M2 was low, that of M3 was moderate and there was very little difference in predictive quality between M4 and M5. Mixing the two field- and UAV-based variables (M3) explained growth variance 40% better than models M1 and M2, which contained only one type of variable (Fig. 4), and reduced the MSPE of these models by at least 17% (Fig. 3a). The maximum R^2 adj was obtained using all possible variables (M5, Table 2). However, with an R^2 adj better than that of M3 (Fig. 4b,c) and representing 90% of that of M5, M4 had the advantage of not containing the DBH-based competition indices, and therefore of containing fewer variables than the other two models. Going from M4 to M5 showed that adding DBH-based competition indices to a model already containing tree size variables and crown-based competition indices improved growth predictions very slightly. The relative gain in R^2 adj varied from 0.6% to 1.4% (Fig. 4b,c) and the reduction in harmonic mean of the mean square prediction error (MSPE) was 0.8% (Fig. 3a).

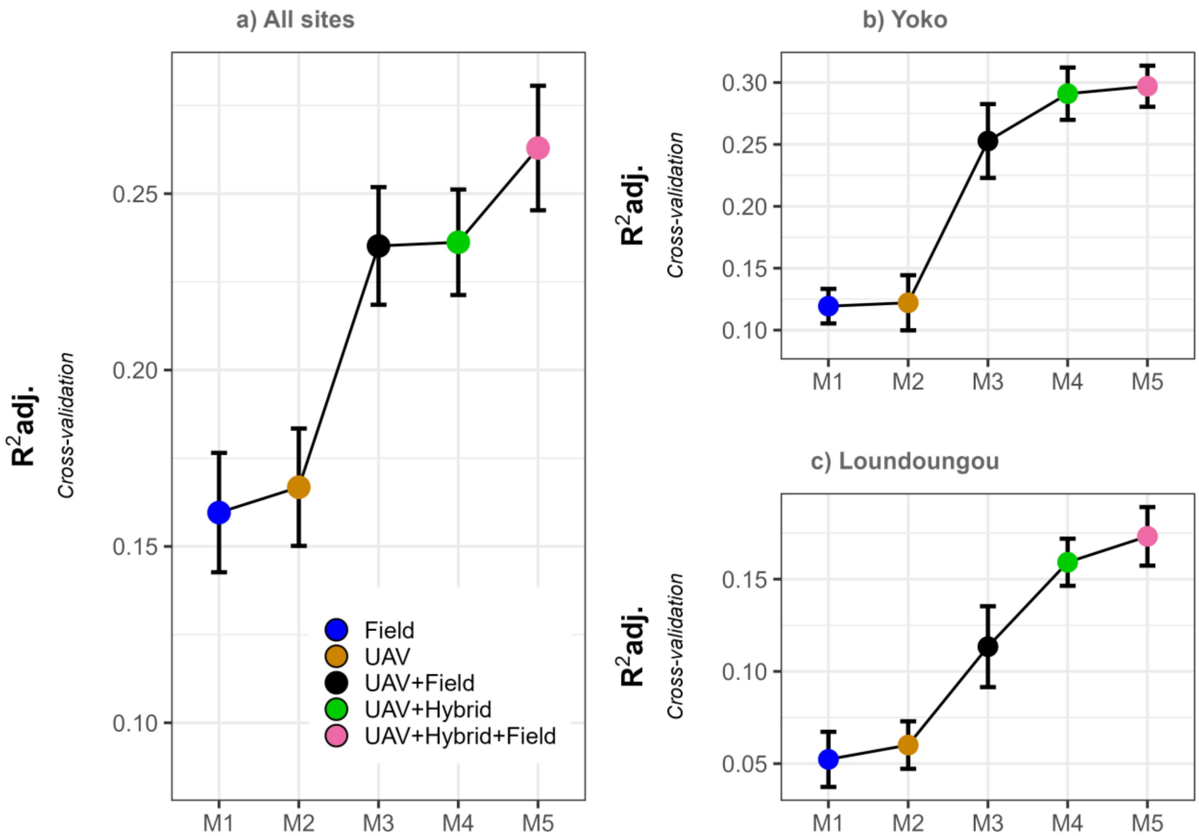

Fig. 4. Adjusted coefficient of determination of the different growth models calibrated using M1 (field variables), M2 (UAV variables), M3 (mixture of field and UAV variables), M4 (tree diameter, UAV and hybrid variables), and M5 (set of all measured variables). Mean R^2adj values supplemented by the standard deviation are presented for each model.

Linear regression showed that the ratio of crown area to basal area (hybrid variable) explained 15% (AIC = 112.1, RSE = 0.256, $p < 0.001$) of the variability in diameter increment (DBHI) at both sites. Together with species guild, variables characterizing tree size (DBH, CA, CBR) explained 20% of diameter increment (AIC = 49.27, RSE = 0.247, $p < 0.001$). The M4 model, containing the crown-based CIs in addition to tree dimensions, was significantly better ($F = 9.60$, $p < 0.001$) than without these CIs. As with the SCGLR models, comparison of the linear models

M4 (R^2 adj = 0.246, AIC = 4.738, RSE = 0.241) and M5 (R^2 adj = 0.256, AIC = −4.690, RSE = 0.239) in Table 5 shows that adding diameter-based CIs to a model already containing tree dimensions and crown-based CIs marginally improved the quality of DBHI predictions (Table 5). Results also showed that both asymmetric (CAH, NCL) and symmetric (NCA, NCI) crown indices were significant in growth models (Table 5). Without significant effect, the site did not appear to be a relevant variable in the two models M4 and M5. Models containing the site variable were not significantly different from those that did not contain it, whether they were of type M4 (F = 1.719, P = 0.19) or M5 (F =0.646, P =0.422).

*Table 5. Estimated coefficients of the linear models (M4 and M5) using the trees located inside the core zones in both sites (n = 984). M5 contains all possible variables from the field, UAV and hybrids. M4 contains the variables from M5 except for the competition indices from the field data. The reference factor level for the species guild is "shade bearer". Significance of parameters is indicated at the statistical threshold of 0.05: *, 0.01: ** and 0.001: ***. R^2 adj is the coefficient of determination of the fitted model. RSE is the residual standard error.*

		M4					M5				
			R^2 adj	AIC	df	RSE		R^2 adj	AIC	df	RSE
			0.246	4.738	973	0.241		0.256	-4.690	969	0.239
Variables	Predictor	Estim.	SE	*t*	*p*	Sign.	Estim.	SE	*t*	*p*	Sign.
	Intercept	-0.858	0.150	-5.710	0.000	***	-0.828	0.160	-5.178	0.000	***
Hybrid	CBR	0.189	0.015	12.471	0.000	***	0.189	0.002	10.814	0.000	***
TE	NPLD	0.032	0.018	1.812	0.070		0.038	0.018	2.162	0.031	*
	Pioneer	0.210	0.025	8.521	0.000	***	0.214	0.025	8.702	0.000	***
	CD	-0.010	0.004	-2.844	0.005	**	0.014	0.002	6.041	0.000	***
	ΔALT_10	0.014	0.002	5.952	0.000	***	0.009	0.002	4.193	0.000	***
UAV	CAH_5	0.000	0.000	2.919	0.004	**	0.000	0.000	2.759	0.006	**
	NCA_15	-0.000	0.000	-4.305	0.000	***	-0.000	0.000	-4.112	0.000	***
	NCL_20	0.005	0.003	1.651	0.099		-0.007	0.003	2.352	0.019	*
	NCI_25	0.498	0.172	2.896	0.004	**	0.453	0.172	2.644	0.008	**

	BAR_10	-	-	-	-	-	5.9e7	2.9e7	2.038	0.042	*
Field	NnT_10	-	-	-	-	-	-0.020	0.007	-2.838	0.005	**
	SBA_10	-	-	-	-	-	-18.900	9.228	-2.048	0.041	*
	SBAT_10	-	-	-	-	-	0.121	0.050	2.638	0.008	**

3.3 Between-site differences

The most important variables for predicting growth were similar at both sites as indicated by the results of M4 (Fig. 5). However, their relative influence on growth was variable. In particular, crown-based variables and DBH predicted tree growth better at Yoko (R^2 adj = 0.34, AIC = −164.5) than at Loundoungou (R^2 adj = 0.20, AIC = 64.6). The position of the crown distinguishing dominated trees from dominant trees did not appear in the final model calibrated at Yoko.

Testing a model calibrated at one site to predict growth at the other site gave an explained variance comparable to that obtained with locally calibrated models (Table 6, comparison of results in (a) versus (b), results in (c) versus (d)). Analysis of residuals showed the validity of prediction models from one site to the other (see Appendix F). The final models contained the stem size class variable, distinguishing small trees (DBH < 40 cm) from large trees (DBH ≥ 40 cm). In all local models, the coefficients associated with small trees were significantly positive.

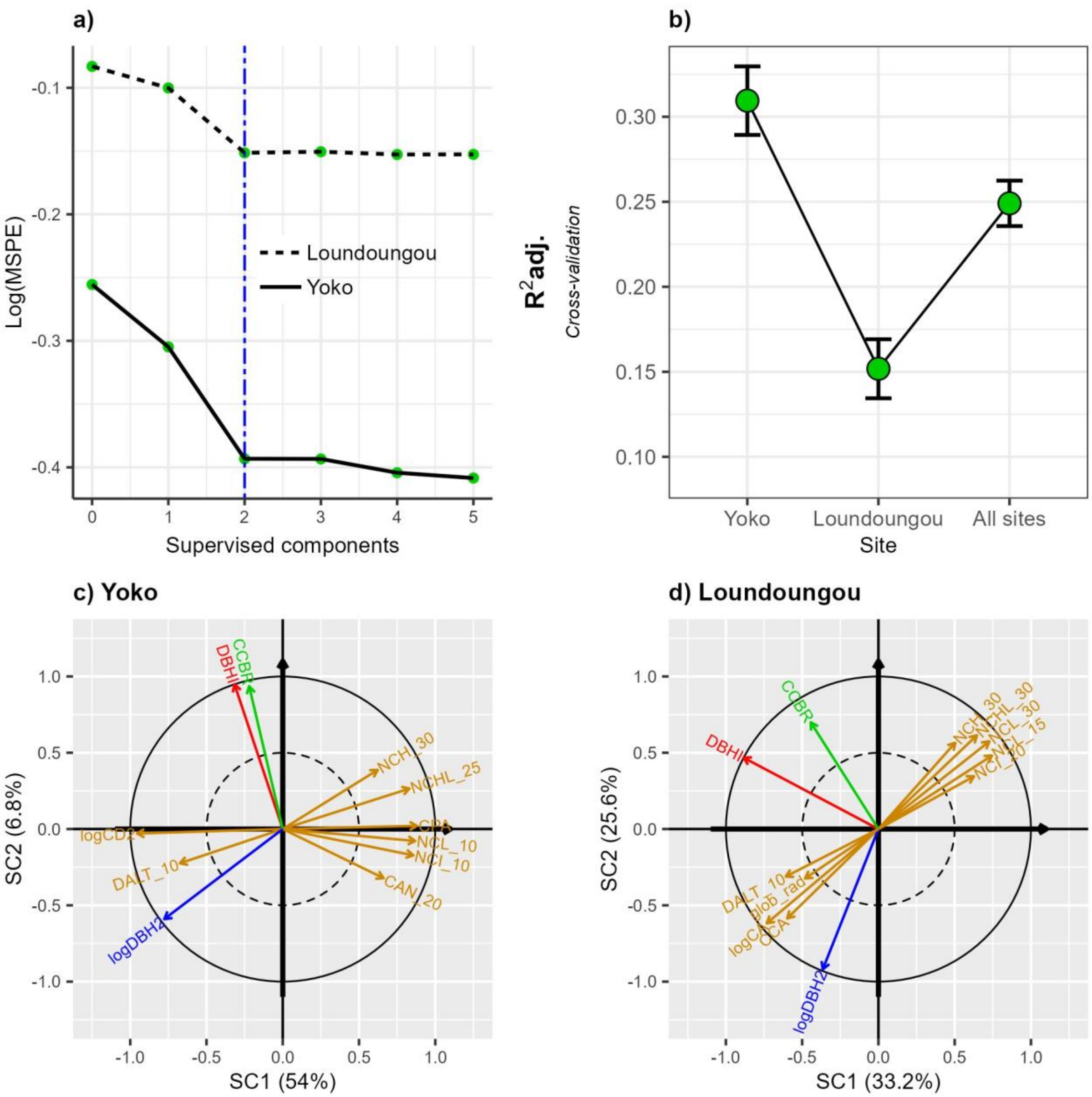

Fig. 5. Results of using the M4 model tested at each of the two sites. Since M4 did not include DBH-based competition indices, this model was fitted again using data from the trees located in the core and the edge zones of the plots (Fig. 2a). The number of optimal components is marked by the blue dotted lines in (a), and the R^2 adj values are shown in (b). The correlation plots of the variables in the planes formed by the supervised components are presented in (c) for the Yoko site (n = 876) and in (d) for the Loundoungou site (n = 682). In the plots, the response variable is shown in red, DBH-based explanatory variables in blue,

UAV-based explanatory variables in orange and hybrid variables in green. The parameters used for the fits are $s = 0.14$, $l = 7$ in Yoko, and $s = 0.18$, $l = 7$ in Loundoungou.

Table 6. Coefficients of the SCGLR models calibrated at each site and tested alternatively to predict growth at the second site. The reference factor level for species guild was "shade tolerant". The reference factor level for the “crown situation” variable was "dominant trees". The reference factor level for the “stem size class” variable was "large trees". Significance of parameters is indicated at the statistical threshold of 0.05: *, 0.01: ** and 0.001: ***. R^2 adj is the adjusted coefficient of determination. RSE is the residual standard error. Parameter values were replaced by “—” for the variables that were not selected in the final model.

	(a) Model calibrated at Yoko				(b) Loundoungou model tested at Yoko			
	n	R^2 adj	AIC	RSE	*n*	R^2 adj	AIC	RSE
	876	0.34	-164.5	0.219	876	0.33	-145.2	0.222
	Est.	RSE	*t*	*p*	Est.	RSE	*t*	*p*
Intercept	0.211	0.012	17.407	0.000***	0.202	0.013	15.021	0.000***
SC1	–0.005	0.002	–3.338	0.000***	–0.041	0.005	–8.507	0.000***
SC2	0.044	0.005	9.533	0.000***	0.018	0.005	3.586	0.000***
Pioneer	0.278	0.026	10.728	0.000***	0.237	0.028	8.462	0.000***
NPLD	0.071	0.017	4.238	0.000***	0.054	0.017	3.208	0.001**
Small trees	0.125	0.025	5.026	0.000***	0.162	0.026	6.300	0.000***
Dominated trees	—	—	—	—	0.027	0.020	1.369	0.171

	(c) Model calibrated at Loundoungou				(d) Yoko model tested at Loundoungou			
	n	R^2 adj	AIC	RSE	*n*	R^2 adj	AIC	RSE
	682	0.20	64.6	0.252	682	0.17	93.9	0.258
	Est.	RSE	*t*	*p*	Est.	RSE	*t*	*p*
Intercept	0.341	0.017	20.091	0.000***	0.345	0.017	19.718	0.000***
SC1	–0.045	0.006	–7.630	0.000***	–0.004	0.002	–2.240	0.025*
SC2	0.020	0.006	3.411	0.000***	0.041	0.007	6.138	0.000***
Pioneer	0.101	0.028	3.570	0.000***	0.153	0.028	5.564	0.000***
NPLD	0.004	0.022	0.194	0.846	0.021	0.022	0.944	0.346
Small trees	0.063	0.032	1.928	0.054	0.033	0.033	0.988	0.324
Dominated trees	–0.039	0.028	–1.312	0.190	–0.094	0.028	–3.345	0.000***

4. DISCUSSION

Aerial imagery offers the potential to derive relevant tree crown information and so obtain more accurate estimates of tropical tree growth (Tompalski et al., 2021). Tree crown information from UAV data can produce good predictors of the growth of upper and lower canopy trees (Guerra-Hernández et al., 2017). Adding such predictors to tree growth models that already include variables measured by field monitoring was found to improve model R^2 adj by a factor of two.

Stem diameter (from field monitoring) and crown measurements (from UAV monitoring) were found to be complementary variables. Moreover, in the models that included the effects of tree size (DBH, crown area) and crown-based competition indices, diameter-based competition indices were no longer relevant for predicting tree growth. Tree competition could thus be assessed with UAV data without requiring additional data from field surveys. Focusing on modelling crown competition, the best model for both sites contained similar variables, suggesting that a general model of tree growth in tropical forests could be fitted with larger datasets. To the best of our knowledge, our study presents pioneering results of crown competition analysis based on the characterization of tropical forest canopy structure using UAV technology.

4.1 Remote sensing provides data complementary to field data

Estimating the growth of tropical trees using remote sensing is valuable because it reduces the need for labor-intensive field data collection. We found that the amount of explained variance was similar using field data and remotely sensed data. Although these results did show an interesting potential for UAV data, we had expected them to provide even better predictions, because such measurements can be used to assess the availability of light at the tree scale, one of the main factors limiting tropical tree growth (Baker et al., 2003). The UAV data likely emerged as limited predictors of tree growth because only the crown of dominant or co-dominant trees could be identified on aerial images. All the study trees had their crowns almost entirely exposed to light, limiting the variability of the computed competition indices. Moreover, crown competition assessed by remote sensing does not fully reflect the competition the tree experiences. Factors such as root competition for water and nutrients, which are important determinants of growth (West, 2023), remain challenging to quantify through photogrammetric measurements. In contrast, competition indices based on field measurements can provide some insight into root competition, as they supply information on all neighboring trees. This likely explains the observed complementarity between UAV measurements of tree crowns and field measurements of tree diameter.

The best model of tree growth combined UAV data with field-measured stem diameter. This model fit was satisfactory (R^2 adj = 0.26) and 40% better than the model containing only field-based variables (R^2 adj = 0.15) or UAV-based variables (R^2 adj = 0.17). These two data sources were thus complementary, similar to previous findings in both tropical forests (Ndamiyehe et al., 2020) and temperate forests (Wyckoff and Clark, 2005). Similarly, the hybrid variable calculated from DBH and crown area (the ratio of crown area to tree basal area) was found to be the best predictor of tree growth in both sites, explaining 15% of the predicted variance (Fig. 3e,f and Fig. 5c,d). This result confirms that tree growth depends on tree architecture (Hérault et al., 2011), tree dimensions reflecting metabolic capacity (West and Ratkowsky, 2021) and resource availability with a larger illuminated crown having higher growth at a given DBH (Baker et al., 2003; Schomaker et al., 2007; Wyckoff and Clark, 2005). The explanatory power of the hybrid variable and its positive correlation with diameter growth suggest that such variables are good indicators of tree competition and tree life history. Indeed, once a tree reaches the canopy, it can change its resource allocation strategy allocating more resources to lateral crown expansion and less resources to height growth (Antin et al., 2013; Blanchard et al., 2016). Hybrid variables may better capture this effect than the other tested variables.

The variance explained in our growth models (~25%) was greater than that often reported in tropical rainforest. Notably, it was twice that of the models established in the Panama rainforest

(12%) using DBH and light availability measurements (Rüger et al., 2011). It was also higher than that explained by models of Adame et al. (2014) in the Puerto Rico forest (15%) comprising the effects of tree characteristics (DBH, height, social status), diameter-based CIs, and species guild. The relatively good performance of our models is partly due to the contribution of crown measurements obtained with UAVs, which are generally lacking in other studies. It is also attributable to the fact that our study focuses on large trees, whereas existing models in tropical forests are generally fitted on all trees with DBH ≥ 10 cm (i.e., with datasets containing many small trees). In addition, the use of component-based regressions keeps more variables in the models, even redundant ones, letting each of them contribute maximally to prediction (Bry et al., 2013).

The use of diameter-based CIs appeared of limited relevance when UAV data and DBH were available. Most asymmetrical competition indices obtained from field or UAV data were closely correlated. In particular, the number or basal area of neighbors taller than the subject tree (SBAT, NnT) were strongly correlated with the number or area of neighboring crowns higher and larger than the subject (NCHL, CALH), with r reaching 0.7 ($p < 0.001$). Additionally, even though symmetrical competition indices from the two data sources showed weaker correlations ($r \leq 0.4$), they were still significantly correlated. Thus, the contribution of diameter-based CIs to explaining growth in a model that already contains crown-based CI was low, suggesting that crown-based CIs can replace DBH-based CIs. This result has practical implications for inventory work, as it shows that remote sensing, in this case by UAV, can reduce the workload of traditional inventories. By eliminating the need for field competition indices in growth models, the systematic positioning and measurement of small-diameter trees (DBH < 40 cm) is no longer essential for estimating the growth of canopy trees if UAV data can be obtained more readily.

Small trees were found to grow faster than large trees (DBH ≥ 40 cm, Table 6). It should be noted that the small trees were mostly detected and thus sampled in canopy gaps where they faced less light competition from the large trees. The threshold of 40 cm (DBH class 30-40 cm) can also represent the ontogenetic stage at which many species reach their maximum growth rate (Hérault et al., 2011). These two reasons might explain why small trees were found to have higher diameter increments than larger trees.

4.2 Effects of crown competition indices

Different crown competition indices were built from UAV data to predict tree growth. The performance of these predictors was generally significant, complementary to the indices built from field survey but limited. Tree growth was generally negatively correlated to crown-based competition indices as expected and in line with what is generally observed with diameter-based CIs across tropical forests (Barros de Oliveira et al., 2021; Rozendaal et al., 2020).

Nevertheless, crown-based CIs explained a relatively small proportion of the variance of diameter growth. Adding them to a model containing tree size variables improved model fits by only 2%. The smallness of the contribution made by competition-based measures to explaining growth was nevertheless not surprising in tropical forests (Barros de Oliveira et al., 2021; Gourlet-Fleury et al., 2023; Laurans et al., 2014). It can be explained by the fact that the intrinsic characteristics of the tree (i.e., its diameter and crown size) already integrate the effects of past competition (Prévosto, 2005). The effect of tree size can hardly be distinguished from that of competition (West and Ratkowsky, 2021), but see Rüger et al. (2011) for an approach disentangling size and light response at species level. It can also be explained by the low power of competition indices to predict tree growth in tropical forests owing to high species diversity with sharply contrasting responses to light conditions, and high interspecific growth variation (Barros de Oliveira et al., 2021; Charbonnier et al., 2017; Rozendaal et al., 2020; Rüger et al., 2011). In particular, the low gradient of light availability for dominant trees sampled also likely explains, at least partly, the limited contribution of the crown-based CI for growth predictions. Future studies could additionally include indices of tree vigor such as the ratio of living crown length (Stăncioiu et al., 2021) or the degree of crown fragmentation (Rutishauser et al., 2011). Such indices might appear useful to further investigate the interaction between tree architecture, resulting partly from the competition history, and tree growth.

Both asymmetric and symmetric crown indices significantly explained tree growth, indicating their complementarity and the importance of using them simultaneously as it has already been recommended (Sun et al., 2019). The best important asymmetric competition indices corresponded to numbers and area of neighboring crowns taller or wider than the subject tree. Ma et al. (2018) also tested similar crown indices to predict tree growth in temperate forests. In particular, they found that the index related to the number of taller crowns quantified with LiDAR data was more closely correlated with the volume growth of conifer tree crowns.

Delimiting the zone of influence to accurately assess competition experienced by a subject tree remains challenging in tropical forests. Several approaches have been used, including the fixed radius method (Gourlet-Fleury and Houllier, 2000; Gourlet-Fleury et al., 2023) and the crown overlap method (Zambrano et al., 2019). In this study, we calculated indices with a varying radius. Our results show that the indices contained in the best models were associated with zones of influence with a radius in the range 5–30 m, suggesting that a single radius does not fully capture the effect of competition (Zambrano et al., 2019).

In this study, we propose a new approach to determine the social status of trees using UAV that is comparable to the classic Dawkins index (Dawkins, 1958). By comparing the altitude of the target tree with that of its neighbors (ΔALT), we could define whether the tree was dominant or dominated. Contrary to the Dawkins index based on a partly subjective estimate, ΔALT has the advantage of being a continuous quantitative variable that can be easily measured for the trees whose crowns are often hardly visible from the ground (Laurans et al., 2014). ΔALT was a significant predictor of tree growth ($p < 0.001$) with dominant trees showing, as expected, more sustained growth than less dominant trees (Moravie et al., 1999). The magnitude of this effect depends, however, on the sampled gradient of ΔALT and significant effect could likely only be observed when the sampled gradient is not too limited (Ndamiyehe et al., 2020). Further studies could test whether ΔALT variable can substitute for the Dawkins index fitting growth models including one or the other indicator of social status.

4.3 Developing a general tree growth model with UAV data

A general tree growth model would be useful for predicting tree growth across a wide range of species and environmental conditions. In our study, we found that the best models for both sites contained similar variables: DBH, crown size, and crown-based CIs. Additionally, a model calibrated at one site to predict growth at the other, and vice versa, showed predictions comparable to those of the local models. Furthermore, the site effect did not appear significant in models containing all the trees from Loungoungou and Yoko. This effect was likely limited when the effect of the other explanatory variables was already taken into account and the site effect could have been partly captured by the other explanatory variables. It suggests that a general model might be devised for multiple sites. However, predicted growth variance was better explained for trees growing at Yoko than at Loundoungou, probably because of the varied growth conditions in the two sites, marked by differences in canopy structure, soil, and climatic characteristics (Gourlet-Fleury et al., 2023). Similar variation in predicted variance between sites of growth models based on crown measurements was also reported by Ma et al. (2018) in temperate forests. In their case, model performance varied with tree development stage and the abundance of trees belonging to different shade tolerance classes. In our study, we observed that crown measurements predicted tree growth better in the site with the highest stand density (~450 stems ha^{-1}). To fit a general model for a large-scale use, further studies will particularly need to investigate the effects of canopy structures, crown density, and environmental conditions. Moreover, the species composition in our two study sites was contrasted with more individuals of shade-tolerant species at Yoko (n = 512) than at Loundoungou (n = 324). In future studies, it would be interesting to analyze to what extent species composition can affect DBH growth predictions from UAV images. This would however require data collected in a larger number of sites.

4.4 Practical implications and remaining challenges

UAV technology, with its ability to produce high-resolution images, allows detailed descriptions of canopy structure, which are essential for a better understanding of how forest ecosystems work. In this study, orthoimages with a resolution of 10 cm pixel^{-1} and DSM of 30 cm pixel^{-1} enabled us to detect differences in canopy structure at two forest sites. These two sites differed significantly in both size and number of crowns in the canopy, with higher crown density but smaller crowns in Yoko than in Loundoungou. These differences in canopy structure were also consistent with differences in stem density observed with field inventories, with nearly 450 stems ha^{-1} at Yoko against 350 stems ha^{-1} at Loundoungou.

Using UAVs to study canopy structure and predict tree growth costs less than other remote sensing methods such as those using LiDAR technology (Dandois and Ellis, 2013). However, its use is only relevant for large trees with crowns in the upper part of the canopy. This UAV approach could be of particular interest for planning logging operations, since most exploitable trees generally have DBH ≥ 40 cm, and high proportions (65–80%) of trees of this size stand out on aerial images of tropical forests (Araujo et al., 2020; Ndamiyehe et al., 2020). Moreover, the UAV's ability to detect the largest trees remains important because large trees preempt the largest share of resources, have pivotal roles in stand dynamics, store high amounts of carbon (Slik et al., 2013; Stephenson et al., 2014). Using UAV can then be an efficient way to assess and monitor key forest components (Bastin et al., 2015).

Manual delineation of tree crowns and co-recording of UAV field data remain a limitation to the use of remote sensing for individual tree growth assessment (Tompalski et al., 2021). In this study, to describe the neighborhood of each tree crown, it was necessary to delineate, from the UAV images, all neighboring tree crowns. This work is time-consuming, especially for dense canopies. Automatic delineation and recognition of tree crowns and species on images is thus necessary to alleviate measuring dendrometry variables from images. Several deep learning techniques have been tested for computer vision of various objects, including trees on UAV images (Ball et al., 2023; Dos Santos et al., 2019; Morales et al., 2018). Although promising results have already been reported for tree crown detection and delineation in plantations (Ocer et al., 2020), in temperate forests (Kattenborn et al., 2019; Schiefer et al., 2020; Yu et al., 2022) as well as in tropical forests (Ball et al., 2023), the use of these techniques to detect species still remains complicated in tropical forests owing to the high specific diversity (Slik et al., 2015) and multi-layered structure of canopies. Further research is needed to adapt these tools to tropical forests and improve them. In this regard, our dataset, which paired tree records from UAV and field data, could be used as a training dataset to develop such tools.

Another remaining challenge is the estimation of tree height: the difficulty detecting "ground" points on images acquired in dense forest makes it difficult to create a digital terrain model and thus to estimate tree height, especially for hill terrains. Among the recommended solutions to solve this problem, we can consider the use of lidar drones, whose cost remains high but has fallen significantly in recent years: solutions are available for about 25,000 €. Integrating height into growth models would probably improve the predictions of tree growth.

5. CONCLUSION

Crown competition indices estimated from UAV photogrammetry capture valuable information to predict tree growth, and this information is complementary to that provided by tree dimensions as classically recorded from field inventory. Most competition indices obtained from field or UAV data were closely correlated. Thus, in a model including the effect of UAV-based crown measurements, the DBH-based competition indices from field measurements were no longer relevant. The model containing DBH, CA and crown-based CIs proved best on both sites. To build a model that can be generalized on a large scale, a larger number of sites with structurally heterogeneous canopies will have to be sampled. Although the use of UAV still presents some technical constraints particularly in tropical forests, our results show that it can improve our understanding of forest dynamics while simplifying and reducing the cost of forest inventories.

6. ACKNOWLEDGEMENTS

This article is dedicated to Sylvie Gourlet-Fleury, who died while the manuscript was being drafted. We acknowledge her valuable contribution to improving the quality of the final version of the article. We are also grateful for financial support from the International Foundation for Science (IFS research grant D615-1), the FORETS project implemented by CIFOR, the Royal Belgian Institute of Natural Sciences (RBINS), and the French embassy in DR Congo. X. Bry, F. Mortier and C. Trottier were partially funded by the GAMBAS project funded by the French National Research Agency (ANR-18-CE02-0025). Historical forest inventory data and UAV images on the study sites (Loundoungou and Yoko) were obtained within the framework of the P3FAC project and were shared with us by CIRAD and Gembloux Agro-Bio Tech.

7. APPENDICES

7.1 Appendix A: Correlation between explanatory variables

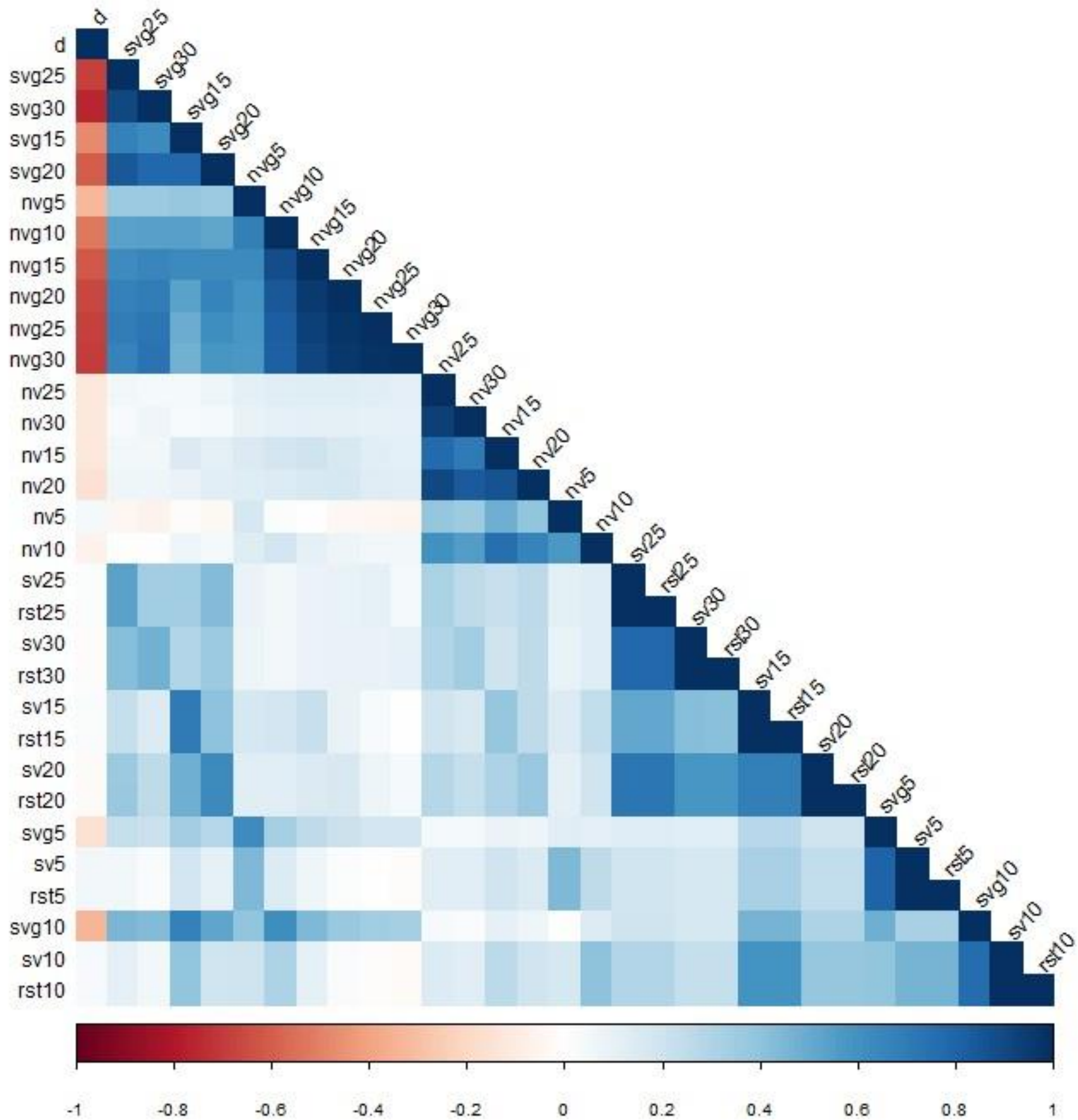

Fig. A.1. Correlation between covariates calculated from field inventory data.

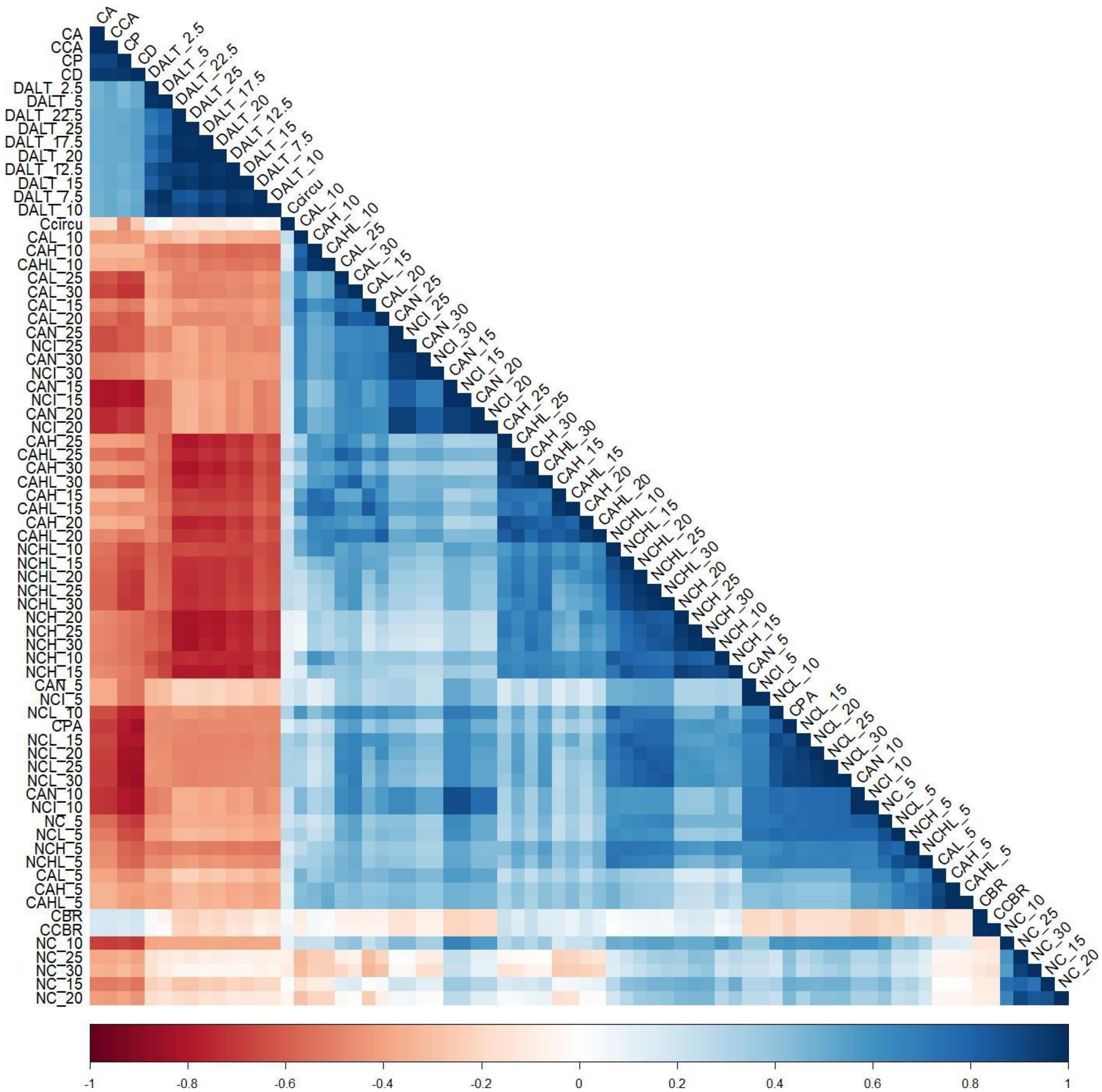

Fig. A.2. Correlation between covariates determined from the UAV data.

7.2 Appendix B: Results from principal component analysis on all explanatory variables

PCA results on the explanatory variables used in this study highlight three main axes. Axis 1 separates trees according to their size expressed by DBH and by crown size (CCA, CP, CD). Small trees lie on the positive side and large trees on the negative side. Axis 1 also shows that tree size is positively correlated with ΔALT variables but negatively correlated with asymmetric competition indices (NCL, NCH, NnT). This indicates that the larger the tree, the less competition it faces from larger and/or taller neighboring trees. Asymmetric competition indices calculated from field and UAV imagery are generally closely correlated (e.g., $r = 0.71$, $p < 0.001$ between NnT_30 and NCHL_30).

Axis 2 separates trees according to the basal area of their neighbors (BAR, SBA), which is opposite to the ratio of crown area to basal area of the tree (CBR, CCBR). This axis shows that the greater the competition around a tree, the smaller the crown to basal area ratio. Axis 3 separates trees according to the number of crowns in their vicinity, expressed in terms of symmetric competition indices. This axis shows that symmetric competition indices from field and UAV data are weakly correlated. The best correlation between the symmetric competition indices calculated using these two types of data is $r = 0.41$ ($p < 0.001$) between Nn_30 and Nc_30. We also see on Axis 3 that when the number of crowns in the vicinity of the subject is high, the sum of the areas covered by crowns of trees taller than the subject is lower.

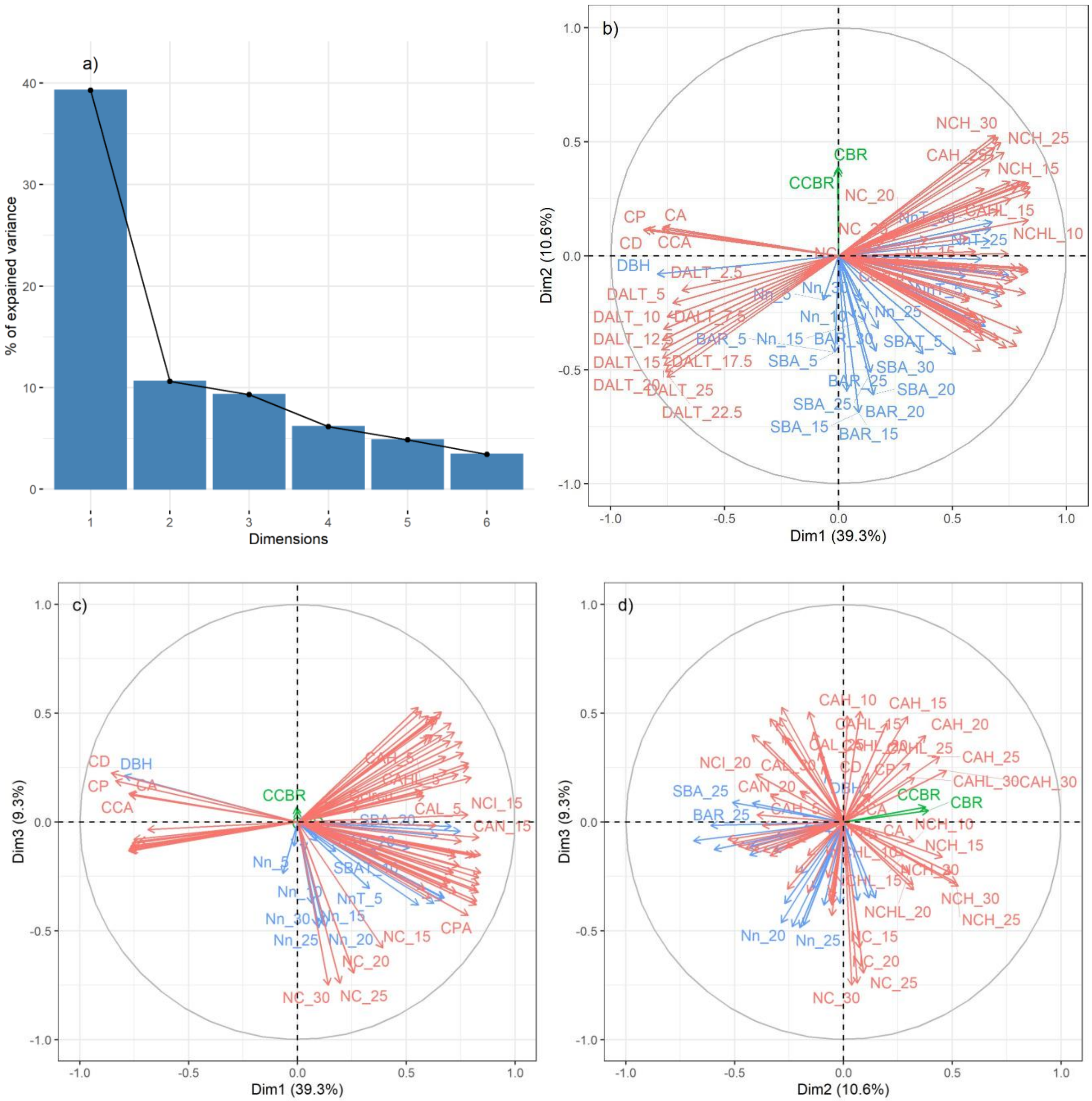

Fig. B.1. Projection of predictor onto the plane formed by the three principal axes of a PCA illustrating the correlations between variables calculated from field data (blue), from UAV data (red), and from hybrid variables (green) derived from these two types of data. The figure shows (a) the histogram of eigenvalues, and (b), (c), and (d) the projection of variables on the first three PCA planes.

7.3 Appendix C: SCGLR model fitting parameters

Table C.1: Parameters l and s and the number k of optimal components of the fitted SCGLR models.

		SCGLR adjustment parameters		
Model	**Data used**	***s***	***l***	***k***
M1	Field	0.18	7	2
M2	UAV	0.18	7	2
M3	UAV + Field	0.18	7	2
M4	UAV + DBH + Hybrid	0.20	7	2
M5	UAV + Field + Hybrid	0.20	7	2

7.4 Appendix D: Distribution of crown size at the two study sites

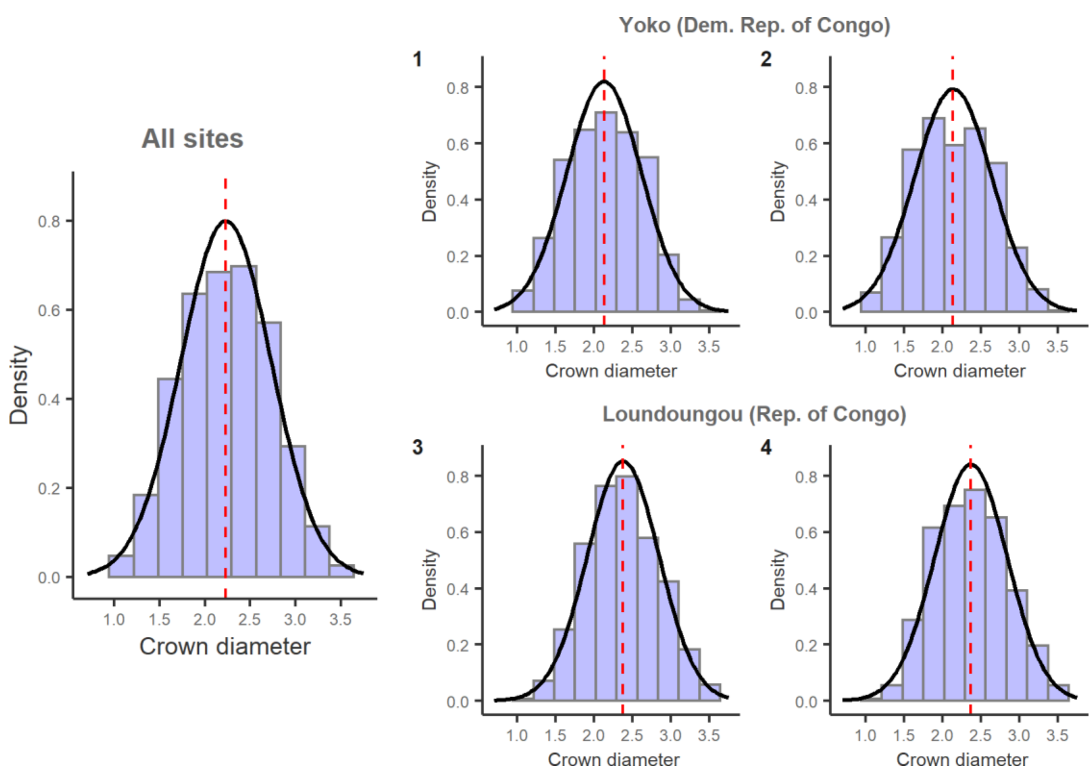

Fig. D.1. Histogram and fitted normal distribution curve of the crown diameter (log-transformed) of the 2630 trees delineated from the orthoimages acquired by UAV at very high resolution. The distributions are presented for both sites combined and for each of the four plots (4 × 9 ha) sampled at *the separate sites: Yoko in DR Congo (n = 1577, for Plot 1 and Plot 2) and Loundoungou in the Republic of Congo (n = 1 053, for Plot 3 and Plot 4). The crown diameter is presented in logarithmic values. Red dotted lines mark the mean for each distribution.*

7.5 Appendix E: Variables that most influenced the supervised components of SCGLR models

Table E.1. Variables with a correlation of absolute value greater than or equal to 0.6 with one of the two supervised components (SC). The variables are distinguished according to the positive (+) or negative (−) sign of their correlation with SC. The sign of the correlation with variable DBHI is also given.

Model	SC	Positive correlation with SC	Negative correlation with SC	Correlation with DBHI
M1	SC1	NnT_30, NnT_25, NnT_20, NnT_15, SBAT_30	DBH, logDBH	(+)
	SC2	-	SBA_15, BAR_15, BAR_20, SBA_20	(+)
M2	SC2	NCL_30, NCL_20, NCL_25, NCL_15, NCI_10, NCL_10, NCA_15, NCI_15, NCHL_20, NCHL_25, NCHL_30, CCA, NCHL_15, NCHL_10, NC_5	CD, CP, CPA, CA, ΔALT_15, logCA, logCD	(-)
	SC2	-	NC_30, NC_25	(+)
M3	SC1	NCL_30, NCL_25, NCL_20, NCI_10, NCA_10, NCL_15, CPA, NCL_10, NCA_15, CCA, NC_5, NCHL_25, NCHL_30, NCHL_20, NCHL_15, NCHL_10, NCL_10, NCA_15, NC_5, NCHL_25, NCHL_30, NCHL_20, NCHL_15, NCHL_10	CD, CP, CCA, ΔALT_10, DBH, logDBH, logCA,	(-)
	SC2	-		(+)
M4	SC1	NCL_30, NCL_25, NCL_20, NCI_10, NCA_10, NCL_15, CPA, NCL_10, NCA_15, NCI_15, NC_5, NCHL_25, NCHL_30, NCHL_20, NCHL_15, NCL_5	CD, CP, CCA, CA, ΔALT_10, logCA, logCD	(-)
	SC2	-	CCBR, CBR	(+)
M5	SC1	NCL_30, NCI_10, NCA_10, CPA, NCL_25, NCL_20, NCL_15, NCA_15, NCI_15, NCL_10,	CD, CP, CCA, CA, logCA,logCD	(-)

		NC_5		
	SC2	-	CAH_20	(+)

7.6 Appendix F: Analysis of residuals from the M4 models applied to the two study sites

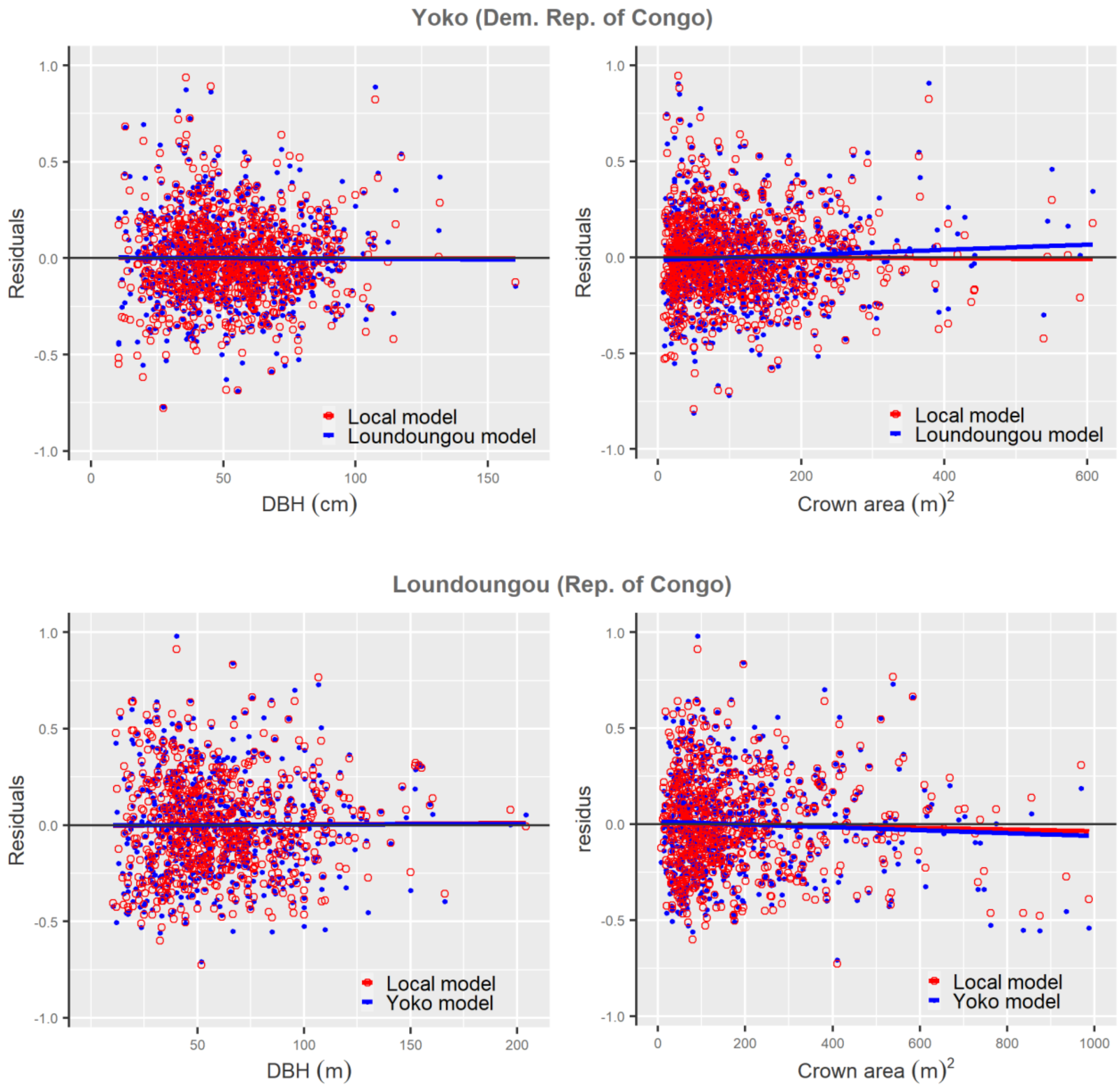

Fig. F.1. M4 model residuals as a function of BBH and tree crown area at study sites.

7.7 Appendix G: Data

The dataset used in this study is provided as an attached file.

7.8 Appendix H : DBH and diameter increment distribution of sampled trees by site and species guild

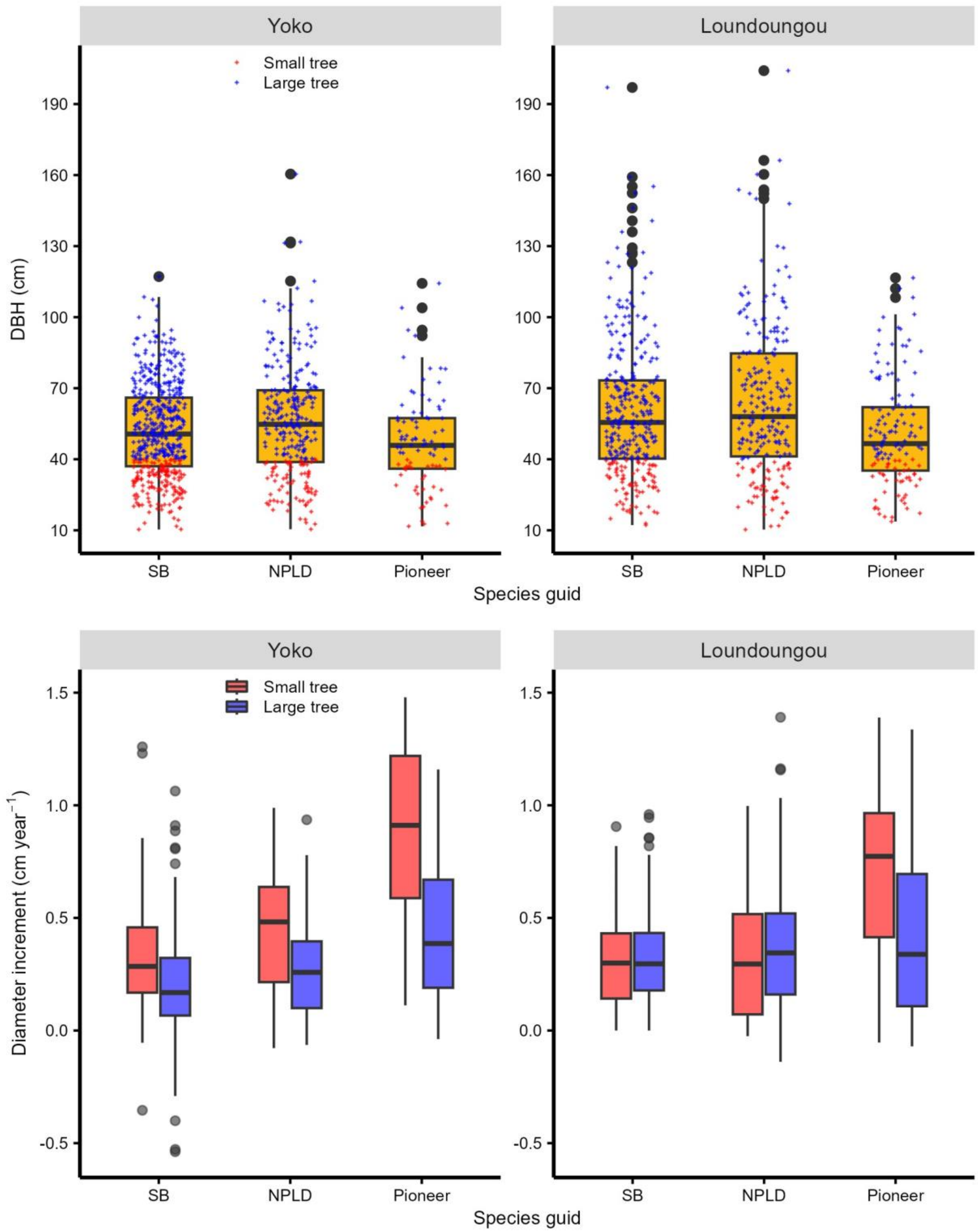

Fig. H.1. Distribution of DBH and diameter increment (DBHI) of the trees co-recorded between the field and UAV measurements, in the two sites, Yoko (n = 876) and Loundoungou (n =682). The distributions are presented by site and by species guild.

8. REFERENCES

Adame, P., Brandeis, T.J., Uriarte, M., 2014. Diameter growth performance of tree functional groups in Puerto Rican secondary tropical forests. For. Syst. 23, 52–63. https://doi.org/10.5424/fs/2014231-03644

Anderson, E.C., Winter, D.J., 2020. Simple Features for R. Package "sf" (version 0.9.2).

Antin, C., Pélissier, R., Vincent, G., Couteron, P., 2013. Crown allometries are less responsive than stem allometry to tree size and habitat variations in an Indian monsoon forest. Trees - Struct. Funct. 27, 1485–1495. https://doi.org/10.1007/s00468-013-0896-7

Araujo, R.F., Chambers, J.Q., Celes, C.H.S., Muller-Landau, H.C., Santos, A.P.. F., Emmert, F., Ribeiro, G.H.P.M., Gimenez, B.O., Lima, A.J.N., Campos, M.A.A., Higuchi, N., 2020. Integrating high resolution drone imagery and forest inventory to distinguish canopy and understory trees and quantify their contributions to forest structure and dynamics. PLoS One 1–16. https://doi.org/10.1371/journal.pone.0243079

Baker, T., Swaine, M., Burslem, D., 2003. Variation in tropical forest growth rates: combined effects of functional group composition and resource availability. Perspect. Plant Ecol. Evol. Syst. 6, 21–36. https://doi.org/10.1078/1433-8319-00040

Ball, J.G.C., Hickman, S.H.M., Jackson, T.D., Koay, X.J., Hirst, J., Jay, W., Archer, M., Coomes, D.A., 2023. Accurate delineation of individual tree crowns in tropical forests from aerial RGB imagery using Mask R-CNN. Remote Sens. Ecol. Conserv. 1–14. https://doi.org/10.1002/rse2.332

Barros de Oliveira, E.K., Rezende, A.V., Mazzei, L., Murta Júnior, L.S., Oliveira Castro, R.V., Neves d'Oliveira, M.V., Barros, Q.S., 2021. Competition indices after reduced impact logging in the Brazilian Amazon. J. Environ. Manage. 281.

https://doi.org/10.1016/j.jenvman.2020.111898

Bastin, J., Barbier, N., Réjou-Méchain, M., Fayolle, A., Gourlet-Fleury, S., Maniatis, D., Haulleville, T. de, Baya, F., Beeckman, H., Beina, D., Couteron, P., Chuyong, G., Dauby, G., Doucet, J.-L., Droissart, V., Dufrêne, M., Ewango, C., Gillet, J.F., Gommadje, C.H., Hart, T., Kavali, T., Kenfack, D., Libalah, M., Malhi, Y., Makana, J.-R., Pélissier, R., Ploton, P., Serkx, A., Sonké, B., Stevart, T., Thomas, D.W., Cannière, C. De, Bogaert, J., 2015. Seeing Central African forests through their largest trees. Nat. Publ. Gr. 1–8. https://doi.org/10.1038/srep13156

Bénédet, F., Doucet, J.-L., Fayolle, A., Gillet, J.-F., Gourlet-Fleury, S., Vincke, D., 2013. CoForTraits, base de données d’information sur les traits des espèces d’arbres africaines. Version 1.0. 2018.

Biging, G.S., 1995. Evaluation of competition indices in individual tree growth models. For. Sci. 41, 360–377. https://doi.org/10.1093/forestscience/41.2.360

Blanchard, E., Birnbaum, P., Ibanez, T., Boutreux, T., Antin, C., Ploton, P., Vincent, G., Pouteau, R., Vandrot, H., Hequet, V., Barbier, N., Droissart, V., Sonké, B., Texier, N., Kamdem, N.G., Zebaze, D., Libalah, M., Couteron, P., 2016. Contrasted allometries between stem diameter, crown area, and tree height in five tropical biogeographic areas. Trees-Structure Funct. 30, 1953–1968. https://doi.org/10.1007/s00468-016-1424-3

Bourgoin, C., Betbeder, J., Couteron, P., Blanc, L., Roux, R. Le, Cornu, G., Reymondin, L., Mazzei, L., Sist, P., 2020. UAV-based canopy textures assess changes in forest structure from long-term degradation. Ecol. Indic. 115, 1–29.

Bry, X., Trottier, C., Verron, T., Mortier, F., 2013. Supervised component generalized linear regression using a PLS-extension of the Fisher scoring algorithm. J. Multivar. Anal. 119, 47–

60. https://doi.org/10.1016/j.jmva.2013.03.013

Burkhart, H.E., Tomé, M., 2012. Modeling forest trees and stands. Model. For. Trees Stands 9789048131, 1–457. https://doi.org/10.1007/978-90-481-3170-9

Caha, J., 2023. Qgis: An extension of package "qgisprocess" providing direct R functions for QGIS functions. Version 0.0.0.9000.

Carrillo, G., 2015. vec2dtransf: 2D Cartesian Coordinate Transformation. R package version 1.1. https://doi.org/https://CRAN.R-project.org/package=vec2dtransf

Charbonnier, F., Roupsard, O., Maire, G., Guillemot, J., Casanoves, F., Lacointe, A., Vaast, P., Allinne, C., Audebert, L., Cambou, A., Clément-vidal, A., Defrenet, E., Duursma, R.A., 2017. Increased light-use efficiency sustains net primary productivity of shaded coffee plants in agroforestry system 1592–1608. https://doi.org/10.1111/pce.12964

Cole, W.G., Lorimer, C.G., 1994. Predicting tree growth from crown variables in managed northern hardwood stands. For. Ecol. Manage. 67, 159–175. https://doi.org/10.1016/0378-1127(94)90014-0

Dandois, J.P., Ellis, E.C., 2013. High spatial resolution three-dimensional mapping of vegetation spectral dynamics using computer vision. Remote Sens. Environ. 136, 259–276. https://doi.org/10.1016/j.rse.2013.04.005

Davies, S.J., 2001. Tree Mortality and Growth in 11 Sympatric Macaranga Species in Borneo. Ecology 82, 920. https://doi.org/10.2307/2679892

Dawkins, H.C., 1958. The management of natural tropical high- forests with special reference to Uganda. Imperial Forestry Institute, University of Oxford. Institute Paper 34, p. 155.

Dos Santos, A.A., Marcato Junior, J., Araújo, M.S., Di Martini, D.R., Tetila, E.C., Siqueira, H.L., Aoki, C., Eltner, A., Matsubara, E.T., Pistori, H., Feitosa, R.Q., Liesenberg, V., Gonçalves, W.N., 2019. Assessment of CNN-based methods for individual tree detection on images captured by RGB cameras attached to UAVS. Sensors (Switzerland) 19, 1–11. https://doi.org/10.3390/s19163595

Fayolle, A., Swaine, M.D., Bastin, J.F., Bourland, N., Comiskey, J.A., Dauby, G., Doucet, J.L., Gillet, J.F., Gourlet-Fleury, S., Hardy, O.J., Kirunda, B., Kouamé, F.N., Plumptre, A.J., 2014. Patterns of tree species composition across tropical African forests. J. Biogeogr. 41, 2320–2331. https://doi.org/10.1111/jbi.12382

Filipescu, C.N., Groot, A., Maclsaac, D.A., Cruickshank, M.G., Stewart, J.D., 2012. Prediction of diameter using height and crown attributes: A case study. West. J. Appl. For. 27, 30–35. https://doi.org/10.1093/wjaf/27.1.30

Foli, E.G., Alder, D., Miller, H.G., Swaine, M.D., 2003. Modelling growing space requirements for some tropical forest tree species. For. Ecol. Manage. 173, 79–88.

Franc, A., Gourlet-Fleury, S., Picard, N., 2000. Une introduction à la modélisation des forêts hétérogènes, ENGREF. ed. Nancy, France.

Getzin, S., Wiegand, K., Schöning, I., 2012. Assessing biodiversity in forests using very high-resolution images and unmanned aerial vehicles. Methods Ecol. Evol. 3, 397–404. https://doi.org/10.1111/j.2041-210X.2011.00158.x

Gourlet-Fleury, S., Houllier, F., 2000. Modelling diameter increment in a lowland evergreen rain forest in French Guiana. For. Ecol. Manage. 131, 269–289. https://doi.org/10.1016/S0378-1127(99)00212-1

Gourlet-Fleury, S.G.-, Rossi, V., Forni, E., Fayolle, A., Allah-, G.L.F., Fidèle, B., Fabrice, B., Boyemba, F., Cornu, G., Doucet, L., Gillet, J.-F., Mazengue, M., Mbasi, M., Hoef, Y. Van, Zombo, I., Freycon, V., 2023. Competition and site weakly explain tree growth variability in undisturbed Central African moist forests. J. Ecol. 00, 1–18. https://doi.org/10.1111/1365-2745.14152

Guerra-Hernández, J., González-Ferreiro, E., Monleón, V.J., Faias, S.P., Tomé, M., Díaz-Varela, R.A., 2017. Use of multi-temporal UAV-derived imagery for estimating individual tree growth in Pinus pinea stands. Forests 8, 1–19. https://doi.org/10.3390/f8080300

Hérault, B., Bachelot, B., Poorter, L., Rossi, V., Bongers, F., Chave, J., Paine, C.E.T., Wagner, F., Baraloto, C., 2011. Functional traits shape ontogenetic growth trajectories of rain forest tree species. J. Ecol. 99, 1431–1440. https://doi.org/10.1111/j.1365-2745.2011.01883.x

Hijmans, R.J., Etten, J. van, Sumner, M., Cheng, J., Bevan, A., Bevan, R., Busetto, L., Canty, M., Forrest, D., Ghosh, A., Golicher, D., Gray, J., Greenberg, J.A., 2020. Raster : Geographic Data Analysis and Modeling (version 3.5-2). Cran 1–249.

Hofierka, J., Suri, M., 2002. The Solar Radiation model for Open Source GIS: implementation and applications, in: Proceedings of the Open Source GIS - GRASS Users Conference 2002. Trento, Italy, p. 20.

Järnstedt, J., Pekkarinen, A., Tuominen, S., Ginzler, C., Holopainen, M., Viitala, R., 2012. Forest variable estimation using a high-resolution digital surface model. ISPRS J. Photogramm. Remote Sens. 74, 78–84. https://doi.org/10.1016/j.isprsjprs.2012.08.006

Kattenborn, T., Eichel, J., Fassnacht, F.E., 2019. Convolutional Neural Networks enable efficient , accurate and fine- grained segmentation of plant species and communities from high-resolution UAV imagery. Sci. Rep. 1–10. https://doi.org/10.1038/s41598-019-53797-9

Kunstler, G., Falster, D., Coomes, D.A., Hui, F., Kooyman, R.M., Laughlin, D.C., Poorter, L., Vanderwel, M., Vieilledent, G., Wright, S.J., Aiba, M., Baraloto, C., Caspersen, J., Cornelissen, J.H.C., Gourlet-Fleury, S., Hanewinkel, M., Herault, B., Kattge, J., Kurokawa, H., Onoda, Y., Peñuelas, J., Poorter, H., Uriarte, M., Richardson, S., Ruiz-Benito, P., Sun, I.F., Ståhl, G., Swenson, N.G., Thompson, J., Westerlund, B., Wirth, C., Zavala, M.A., Zeng, H., Zimmerman, J.K., Zimmermann, N.E., Westoby, M., 2016. Plant functional traits have globally consistent effects on competition. Nature 529, 204–207. https://doi.org/10.1038/nature16476

Laurans, M., Hérault, B., Vieilledent, G., Vincent, G., 2014. Vertical stratification reduces competition for light in dense tropical forests. For. Ecol. Manage. 329, 79–88. https://doi.org/10.1016/j.foreco.2014.05.059

Ligot, G., Gourlet-fleury, S., Dainou, K., Gillet, J., Rossi, V., Mazengu, M., Nna, S., Serge, Y., Zombo, I., Forni, E., Doucet, J., 2022. Tree growth and mortality of 42 timber species in central Africa. For. Ecol. Manage. 505, 13. https://doi.org/10.1016/j.foreco.2021.119889

Lisein, J., Linchant, J., Lejeune, P., 2013. Aerial surveys using an Unmanned Aerial System (UAS): comparison of different methods for estimating the surface area of sampling strips 6, 506–520.

Loubota Panzou, G.J., Ligot, G., Gourlet-Fleury, S., Doucet, J.L., Forni, E., Loumeto, J.J., Fayolle, A., 2018. Architectural differences associated with functional traits among 45 coexisting tree species in Central Africa. Funct. Ecol. 1–11. https://doi.org/10.1111/1365-2435.13198

Ma, Q., Su, Y., Tao, S., Guo, Q., 2018. Quantifying individual tree growth and tree competition using bi-temporal airborne laser scanning data: a case study in the Sierra Nevada Mountains, California. Int. J. Digit. Earth 11, 485–503. https://doi.org/10.1080/17538947.2017.1336578

Messinger, M., Asner, G.P., Silman, M., 2016. Rapid Assessments of Amazon Forest Structure and Biomass Using Small Unmanned Aerial Systems. Remote Sens. 8, 1–15. https://doi.org/10.3390/rs8080615

Michez, A., Piégay, H., Lisein, J., Claessens, H., Lejeune, P., 2016. Classification of riparian forest species and health condition using multi-temporal and hyperspatial imagery from unmanned aerial system. Environ. Monit. Assess. https://doi.org/10.1007/s10661-015-4996-2

Morales, G., Kemper, G., Sevillano, G., Arteaga, D., Ortega, I., Telles, J., 2018. Automatic segmentation of Mauritia flexuosa in unmanned aerial vehicle (UAV) imagery using deep learning. Forests 9. https://doi.org/10.3390/f9120736

Moravie, M.-A., Durand, M., Houllier, F., 1999. Ecological meaning and predictive ability of social status, vigour and competition indices in a tropical rain forest (India). For. Ecol. Manage. 117, 221–240. https://doi.org/10.1016/S0378-1127(98)00480-0

Mortier, F., Chauvet, J., Trottier, C., Cornu, G., Bry, X., 2017. La régression linéaire généralisée sur composantes supervisées et ses extensions. p. 21.

Ndamiyehe, N.J.B., Lejeune, P., Gourlet-Fleury, S., Fayolle, A., Mianda-Bungi, L.N., Ligot, G., 2020. Quantifier les dimensions des houppiers à l'aide d'images aériennes à haute résolution pour estimer l'accroissement diamétrique des arbres dans les forêts d'Afrique centrale. Bois Forets des Trop. 343, 67–81. https://doi.org/10.19182/bft2020.343.a31848

Ocer, N.E., Kaplan, G., Erdem, F., Matci, D.K., 2020. Tree extraction from multi-scale UAV images using Mask R-CNN with FPN. Remote Sens. Lett. 11, 847–856. https://doi.org/10.1080/2150704X.2020.1784491

Olpenda, A.S., Sterenczak, K., Bedkowski, K., 2018. Modeling Solar Radiation in the Forest Using Remote Sensing Data : A Review of Approaches and Opportunities. Remote Sens. 10, 22. https://doi.org/10.3390/rs10050694

Paneque-gálvez, J., Mccall, M.K., Napoletano, B.M., Wich, S.A., Koh, L.P., 2014. Small Drones for Community-Based Forest Monitoring: An Assessment of Their Feasibility and Potential in Tropical Areas. Forests 5, 1481–1507. https://doi.org/10.3390/f5061481

PhotoScan, 2015. Agisoft PhotoScan Manuel de l'utilisateur. Profes- sional Edition, version 1.1.

Picard, N., Boyemba, F., Rossi, V., 2015. Reducing the error in biomass estimates strongly depends on model selection. Ann. For. Sci. 72, 811–823. https://doi.org/10.1007/s13595-014-0434-9

Picard, N., Gourlet-Fleury, S., 2008. Manuel de référence pour l'installation de dispositifs permanents en forêt de production dans le Bassin du Congo. CIRAD-COMIFAC.

Popescu, S.C., Wynne, R.H., Nelson, R.F., 2003. Measuring individual tree crown diameter with lidar and assessing its influence on estimating forest volume and biomass 29, 564–577.

Prévosto, B., 2005. Les indices de compétition en for esterie : exemples d'utilisation, intérêts et limites. Rev. For. Fr. LVII, 413–430.

Price, B., Waser, L.T., Wang, Z., Marty, M., Ginzler, C., Zellweger, F., 2020. Predicting biomass dynamics at the national extent from digital aerial photogrammetry. Int. J. Appl. Earth Obs. Geoinf. 90, 102116. https://doi.org/10.1016/j.jag.2020.102116

Purves, D., Pacala, S., 2013. Predictive Models of Forest Dynamics. Science (80-.). 342, 776–776. https://doi.org/10.1126/science.342.6160.776-d

QGIS Development Team, 2020. QGIS Geographic Information System. Open Source Geospatial Foundation.

R Core Team., 2021. R: A Language and Environment for Statistical Computing (Version 4.1.1). R Foundation for Statistical Computing, Vienna, Austria.

Rasmussen, C.R., Weiner, J., 2017. Modelling the effect of size-asymmetric competition on size inequality: Simple models with two plants. Ecol. Modell. 343, 101–108. https://doi.org/10.1016/j.ecolmodel.2016.10.011

Réjou-Méchain, M., Mortier, F., Bastin, J.F., Cornu, G., Barbier, N., Bayol, N., Bénédet, F., Bry, X., Dauby, G., Deblauwe, V., Doucet, J.L., Doumenge, C., Fayolle, A., Garcia, C., Kibambe Lubamba, J.P., Loumeto, J.J., Ngomanda, A., Ploton, P., Sonké, B., Trottier, C., Vimal, R., Yongo, O., Pélissier, R., Gourlet-Fleury, S., 2021. Unveiling African rainforest composition and vulnerability to global change. Nature 593, 90–94. https://doi.org/10.1038/s41586-021-03483-6

Rio, M. del, Condés, S., Pretzsch, H., 2014. Analyzing size-symmetric vs. size-asymmetric and intra-vs. inter-specific competition in beech (Fagus sylvatica L.) mixed stands. For. Ecol. Manage. 325, 90–98. https://doi.org/10.1016/j.foreco.2014.03.047

Rozendaal, D.M.A., Phillips, O.L., Lewis, S.L., Affum-Baffoe, K., Alvarez-Davila, E., Andrade, A., Aragão, L.E.O.C., Araujo-Murakami, A., Baker, T.R., Bánki, O., Brienen, R.J.W., Camargo, J.L.C., Comiskey, J.A., Djuikouo Kamdem, M.N., Fauset, S., Feldpausch, T.R., Killeen, T.J., Laurance, W.F., Laurance, S.G.W., Lovejoy, T., Malhi, Y., Marimon, B.S., Marimon Junior, B.H., Marshall, A.R., Neill, D.A., Núñez Vargas, P., Pitman, N.C.A., Poorter, L., Reitsma, J., Silveira, M., Sonké, B., Sunderland, T., Taedoumg, H., ter Steege, H., Terborgh, J.W., Umetsu, R.K., van der Heijden, G.M.F., Vilanova, E., Vos, V., White, L.J.T., Willcock, S., Zemagho, L., Vanderwel, M.C., 2020. Competition influences tree growth, but not mortality, across environmental gradients in Amazonia and tropical Africa. Ecology 101, 1–11. https://doi.org/10.1002/ecy.3052

Rüger, N., Berger, U., Hubbell, S.P., Vieilledent, G., Condit, R., 2011. Growth strategies of tropical tree species: Disentangling light and size effects. PLoS One 6. https://doi.org/10.1371/journal.pone.0025330

Rutishauser, E., Barthélémy, D., Blanc, L., Eric-André, N., 2011. Crown fragmentation assessment in tropical trees: Method, insights and perspectives. For. Ecol. Manage. 261, 400–407. https://doi.org/10.1016/j.foreco.2010.10.025

Rutishauser, E., Wagner, F., Herault, B., Nicolini, E.A., Blanc, L., 2010. Contrasting above-ground biomass balance in a Neotropical rain forest. J. Veg. Sci. 21, 672–682. https://doi.org/10.1111/j.1654-1103.2010.01175.x

Schiefer, F., Kattenborn, T., Frick, A., Frey, J., Schall, P., 2020. Mapping forest tree species in high resolution UAV-based RGB-imagery by means of convolutional neural networks. ISPRS J. Photogramm. Remote Sens. 170, 205–215. https://doi.org/10.1016/j.isprsjprs.2020.10.015

Schomaker, M.E., Zarnoch, S.J., Bechtold, W.A., Latelle, D.J., Burkman, W.G., Cox, S.M., 2007. Crown-Condition Classification : A Guide to Data Collection and Analysis.

Slik, J.W.F., Arroyo-Rodriguez, V., Aiba, S.-I., Alvarez-Loayza, P., Alves, L.F., Ashton, P., Balvanera, P., Bastian, M.L., Bellingham, P.J., van den Berg, E., Bernacci, L., da Conceicao Bispo, P., Blanc, L., Bohning-Gaese, K., Boeckx, P., Bongers, F., Boyle, B., Bradford, M., Brearley, F.Q., Breuer-Ndoundou Hockemba, M., Bunyavejchewin, S., Calderado Leal Matos, D., Castillo-Santiago, M., Catharino, E.L.M., Chai, S.-L., Chen, Y., Colwell, R.K., Robin, C.L., Clark, C., Clark, D.B., Clark, D. a., Culmsee, H., Damas, K., Dattaraja, H.S., Dauby, G., Davidar, P., DeWalt, S.J., Doucet, J.-L., Duque, A., Durigan, G., Eichhorn, K. a. O., Eisenlohr, P. V., Eler, E., Ewango, C., Farwig, N., Feeley, K.J., Ferreira, L., Field, R., de Oliveira Filho, A.T., Fletcher, C., Forshed, O., Franco, G., Fredriksson, G., Gillespie, T., Gillet, J.-F., Amarnath, G., Griffith, D.M., Grogan, J., Gunatilleke, N., Harris, D., Harrison, R., Hector, A., Homeier, J., Imai, N., Itoh, A., Jansen, P. a., Joly, C. a., de Jong, B.H.J., Kartawinata, K., Kearsley, E., Kelly, D.L., Kenfack, D., Kessler, M., Kitayama, K., Kooyman, R., Larney, E., Laumonier, Y., Laurance, S., Laurance, W.F., Lawes, M.J., Amaral, I.L. Do, Letcher, S.G., Lindsell, J., Lu, X., Mansor, A., Marjokorpi, A., Martin, E.H., Meilby, H., Melo, F.P.L., Metcalfe, D.J., Medjibe, V.P., Metzger, J.P., Millet, J., Mohandass, D., Montero, J.C., de Morisson Valeriano, M., Mugerwa, B., Nagamasu, H., Nilus, R., Ochoa-Gaona, S., Onrizal, Page, N., Parolin, P., Parren, M., Parthasarathy, N., Paudel, E., Permana, A., Piedade, M.T.F., Pitman, N.C. a., Poorter, L., Poulsen, A.D., Poulsen, J., Powers, J., Prasad, R.C., Puyravaud, J.-P., Razafimahaimodison, J.-C., Reitsma, J., dos Santos, J.R., Roberto Spironello, W., Romero-Saltos, H., Rovero, F., Rozak, A.H., Ruokolainen, K., Rutishauser, E., Saiter, F., Saner, P., Santos, B. a., Santos, F., Sarker, S.K., Satdichanh, M., Schmitt, C.B., Schongart, J., Schulze, M., Suganuma, M.S., Sheil, D., da Silva Pinheiro, E., Sist, P., Stevart, T., Sukumar, R., Sun, I.-F., Sunderand, T., Suresh, H.S., Suzuki, E., Tabarelli, M., Tang, J., Targhetta, N., Theilade, I., Thomas, D.W., Tchouto, P., Hurtado, J., Valencia, R., van Valkenburg, J.L.C.H., Van Do, T., Vasquez, R., Verbeeck, H., Adekunle, V., Vieira, S. a., Webb, C.O., Whitfeld, T., Wich, S. a., Williams, J., Wittmann, F., Woll, H., Yang, X., Adou Yao, C.Y., Yap, S.L., Yoneda, T., Zahawi, R. a., Zakaria, R., Zang, R., de Assis, R.L., Garcia Luize, B., Venticinque, E.M., 2015. An estimate of the number of tropical tree species. Pnas 112, 7472–7477. https://doi.org/10.1073/pnas.1423147112

Slik, J.W.F., Paoli, G., Mcguire, K., Amaral, I., Barroso, J., Bastian, M., Blanc, L., Bongers, F., Boundja, P., Clark, C., 2013. Large trees drive forest aboveground biomass variation in moist lowland forests across the tropics. Glob. Ecol. Biogeogr. 22, 1261–1271. https://doi.org/10.1111/geb.12092

Stăncioiu, P.T., Șerbescu, A.A., Dutcă, I., 2021. Live crown ratio as an indicator for tree vigor and stability of turkey oak (Quercus cerris l.): A case study. Forests 12, 1–12.

https://doi.org/10.3390/f12121763

Stephenson, N.L., Das, A.J., Condit, R., Russo, S.E., Baker, P.J., Beckman, N.G., Coomes, D. a, Lines, E.R., Morris, W.K., Rüger, N., Alvarez, E., Blundo, C., Bunyavejchewin, S., Chuyong, G., Davies, S.J., Duque, A., Ewango, C.N., Flores, O., Franklin, J.F., Grau, H.R., Hao, Z., Harmon, M.E., Hubbell, S.P., Kenfack, D., Lin, Y., Makana, J.-R., Malizia, A., Malizia, L.R., Pabst, R.J., Pongpattananurak, N., Su, S.-H., Sun, I.-F., Tan, S., Thomas, D., van Mantgem, P.J., Wang, X., Wiser, S.K., Zavala, M.A., 2014. Rate of tree carbon accumulation increases continuously with tree size. Nature 507, 90–3. https://doi.org/10.1038/nature12914

Sun, S., Cao, Q. V., Cao, T., 2019. Evaluation of distance-independent competition indices in predicting tree survival and diameter growth. Can. J. For. Res. 49, 440–446. https://doi.org/10.1139/cjfr-2018-0344

Tomaschek, F., Hendrix, P., Baayen, R.H., 2018. Strategies for addressing collinearity in multivariate linguistic data. J. Phon. 71, 249–267. https://doi.org/10.1016/j.wocn.2018.09.004

Tompalski, P., Coops, N.C., White, J.C., Goodbody, T.R.H., Hennigar, C.R., Wulder, M.A., Socha, J., Woods, M.E., 2021. Estimating Changes in Forest Attributes and Enhancing Growth Projections: a Review of Existing Approaches and Future Directions Using Airborne 3D Point Cloud Data. Curr. For. Reports 7, 25–30. https://doi.org/10.1007/s40725-021-00139-6

Uriarte, M., Canham, C.D., Thompson, J., Zimmerman, J.K., 2004. A neighborhood analysis of tree growth and survival in a hurricane-driven tropical forest. Ecol. Monogr. 74, 591–614. https://doi.org/10.1890/03-4031

Venables, B., Ripley, B., Bates, D.M., Hornik, K., Gebhardt, A., Firth, D., 2002. Package ‘MASS’ (version 7.3-54). Mod. Appl. Stat. with S.

West, P.W., 2023. Quantifying effects on tree growth rates of symmetric and asymmetric inter - tree competition in even - aged , monoculture Eucalyptus pilularis forests. Trees 37, 239–254. https://doi.org/10.1007/s00468-022-02341-w

West, P.W., Ratkowsky, D.A., 2021. Problems with models assessing influences of tree size and inter-tree competitive processes on individual tree growth: a cautionary tale. J. For. Res. https://doi.org/10.1007/s11676-021-01395-9

Wyckoff, P.H., Clark, J.S., 2005. Tree growth prediction using size and exposed crown area. Can. J. For. Res. 35, 13–20. https://doi.org/10.1139/x04-142

Yu, K., Hao, Z., Post, C.J., Mikhailova, E.A., Lin, L., Zhao, G., Tian, S., Liu, J., 2022. Comparison of Classical Methods and Mask R-CNN for Automatic Tree Detection and Mapping Using UAV Imagery. Remote Sens. 14, 17. https://doi.org/doi.org/10.3390/rs14020295

Zambrano, J., Fagan, W.F., Worthy, S.J., Thompson, J., Uriarte, M., Zimmerman, J.K., Umaña, M.N., Swenson, N.G., 2019. Tree crown overlap improves predictions of the functional neighbourhood effects on tree survival and growth. J. Ecol. 107, 887–900. https://doi.org/10.1111/1365-2745.13075

Zarnoch, S.J., Bechtold, W.. A., Stolte, K.W., 2004. Using crown condition variables as indicators of forest health. Can. J. For. Res. 34, 1057–1070. https://doi.org/10.1139/x03-277